Renewable and Sustainable Energy Reviews 16 (2012) 3409–3429

Contents lists available at SciVerse ScienceDirect

Renewable and Sustainable Energy Reviews

journal homepage: www.elsevier.com/locate/rser

Formation, potential and abatement of plume from wet cooling towers: A review

S.K. Tyagi[a,*], A.K. Pandey[b], P.C. Pant[c], V.V. Tyagi[d]

[a] Sardar Swaran Singh National Institute of Renewable Energy, Kapurthala 144601, Punjab, India
[b] School of Infrastructure Technology & Resource Management, Shri Mata Vaishno Devi University, Katra 182320, J&K, India
[c] Ministry of New & Renewable Energy (MNRE), Government of India, CGO Complex Block 14, Lodhi Road, New Delhi 110003, India
[d] Centre for Energy Studies, Indian Institute of Technology, Delhi, Hauz Khas, New Delhi 110016, India

ARTICLE INFO

Article history:
Received 27 June 2011
Accepted 29 January 2012
Available online 31 March 2012

Keywords:
Cooling tower
Plume control
Solar collector
Commercial building
Phase change materials

ABSTRACT

In recent years the visible impact of the release from wet cooling tower to the atmosphere has become a matter of greater concern. In the past visible plumes were accepted as the inevitable consequence of industrial activities and a sign of thriving manufacturing industry. Plumes from combustion plant may be visible and colored for a variety of reasons. Some are associated with the combustion process itself, such as excessive quantities of nitrogen dioxide causing a brown tinge to plumes or the release of small particles, and/or aerosols, in the plume which scatter light. These factors can be tackled by modification of the combustion process and the introduction of emission control technology. However, the most common cause of plume visibility, and the reason that chimneys attract public attention, is the presence of condensed water vapor in plumes. In this paper attempt has been made to present an overview of the previous research work on the plume from wet cooling towers, which describes the previous work done of few researchers on the formation, potential and abatement of plumes besides, the numerical analysis of wet cooling towers for a typical set of operating parameters.

Contents

1. Introduction

Cooling towers are widely used to reject the waste heat to the ambient air by means of evaporative cooling. A cooling tower is an enclosed box for the cooling of water through evaporation by direct contact with the ambient air, which is achieved partly by an exchange of latent heat from the water evaporation and partly by a transfer of sensible heat. The wet cooling tower is packed with fill or packing materials that provides the sufficient area for heat and mass transfer and to enhance the heat rejection opportunity. The heat rejection in the wet cooling towers is basically through convection between water droplets and the ambient air, as well as by evaporation which allows small portion of water to evaporate into the flow of ambient air entering the cooling tower through side

* Corresponding author.
E-mail address: sudhirtyagi@yahoo.com (S.K. Tyagi).

1364-0321/$ – see front matter
doi:10.1016/j.rser.2012.01.059

openings. The development of the cooling tower analysis began in the 19th century with the first work carried out by Lewis [1] and was used by Robinson [2] for the first time. Robinson [2] established the general principles, applicable to cooling tower design and derived equations for the designers. They [2] further stated a series of fundamental concepts about the mechanism involved in the transfer of heat between liquid, gases, and on the vaporization of liquid. Merkel [3] used the enthalpy potential as the driving force for air water exchange and assumed a similarity between heat and mass convective transfer by means of Lewis number equal to unity which has been used to date. For several decades, many authors have studied the convection phenomena occurring in cooling towers. Baker and Shrylock [4] developed a detailed explanation of the concept of cooling tower's performance clarifying the assumptions and approximations used by Merkel. Sutherland [5] showed that Merkel's theory leads to an underestimation of tower size by 5–15%. Braun [6] developed a confined method to model the performance of both cooling tower and dehumidifying coils. Based on Merkel's theory, the effectiveness–NTU relationships method has been developed by Braun et al. [7], taking into account the saturated air specific heat used for sensible heat exchanger. In the model, two parameters, air-side and water-side heat transfer coefficients were introduced. The results of this method were compared with numerical solutions of the detailed heat and mass transfer models and experimental results.

In order to investigate the effect of (low) water and air flow rates, Shelton and Weber [8] used a mathematical model based on the performance data of the manufacturer. Lebrun [9] presented the fundamentals of a new simulations toolkit oriented upward simple solutions for primary HVAC equipments. In this toolkit all the maximum possible models are used and each model is described by a conceptual scheme. Bernier [10] presented an unidimensional analysis of the spray type counter flow cooling tower showing the influence of fill height, water retention time, and water flow rate on the performance of the cooling tower. Lebrun and Silva [11] presented an analysis of basic heat and mass transfer processes occurring around a droplet in transient cooling tower. Studies on heat and mass transfer analysis on the cooling tower were also made by Naphon [12], Kloppers and Kröger [13–15], Lees [16], and Smith [17] using different methods.

Under the most unfavorable combination of the ambient conditions, thermal load and topography, such a plume can extend few hundred meters and sometime causes visibility and darkness. The latest literature review about cooling towers shows different options for reducing the visible plume using hybrid cooling towers, wet–dry cooling towers, dry cooling towers and so on, depending on the need and demand. As mentioned by number of researchers wet cooling towers are economically and technically cheap easy to build and need less power to operate as compared to other types of towers. But they do not have any control over the visible plume [18–24].

2. Formation, potential and abatement of plume

The ambient air passing through the cooling tower comes into contact with the hot water, takes heat and moisture and exits the tower (Fig. 1) in saturated or superheated state as can be seen clearly in Fig. 2(a). This exhaust leaving the cooling tower remixes with the cooler ambient air and as it cools down the excess moisture condenses in small fog droplets, causing the dense visible plume (white smoke). During winter season, cold, humid ambient air at condition 1 (Fig. 2(a)) is warmed up to condition 2 in the tower, after absorbing the heat released by the hot water and then remixes with the ambient air along the line 2–1. Most of this mixing occurs in the superheated region. Where there is more moisture (such as in

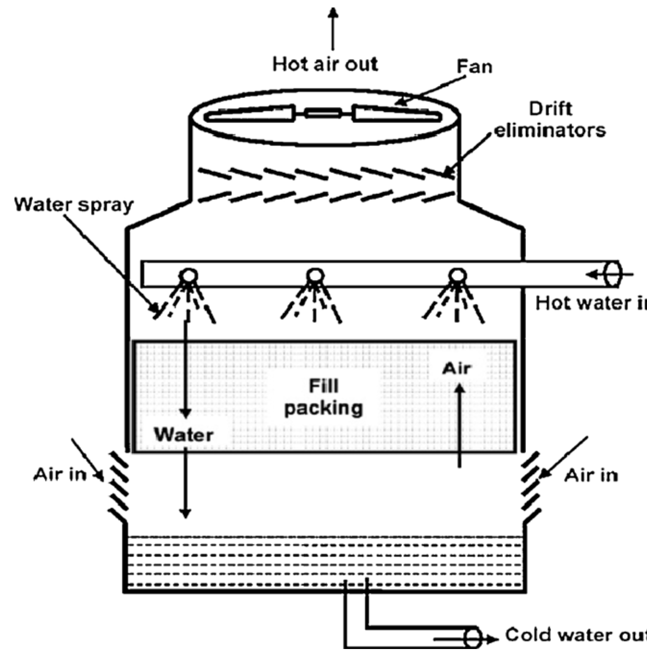


Fig. 1. The working principle of a counter flow cooling tower.

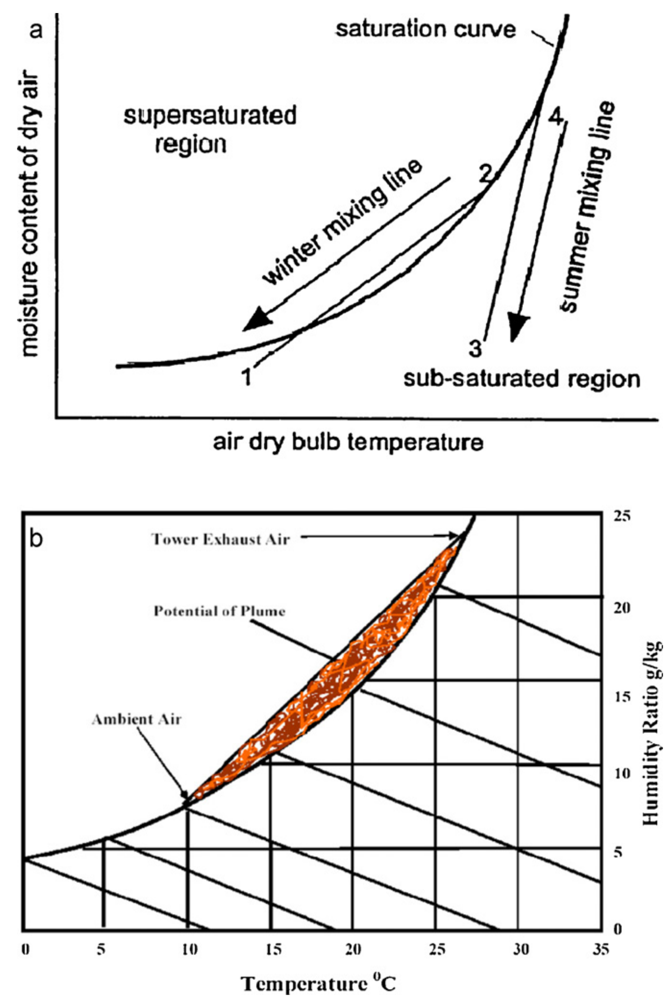


Fig. 2. (a) The formation of plume (fog) in a cooling tower. (b) The potential of plume (fog) in a cooling tower.

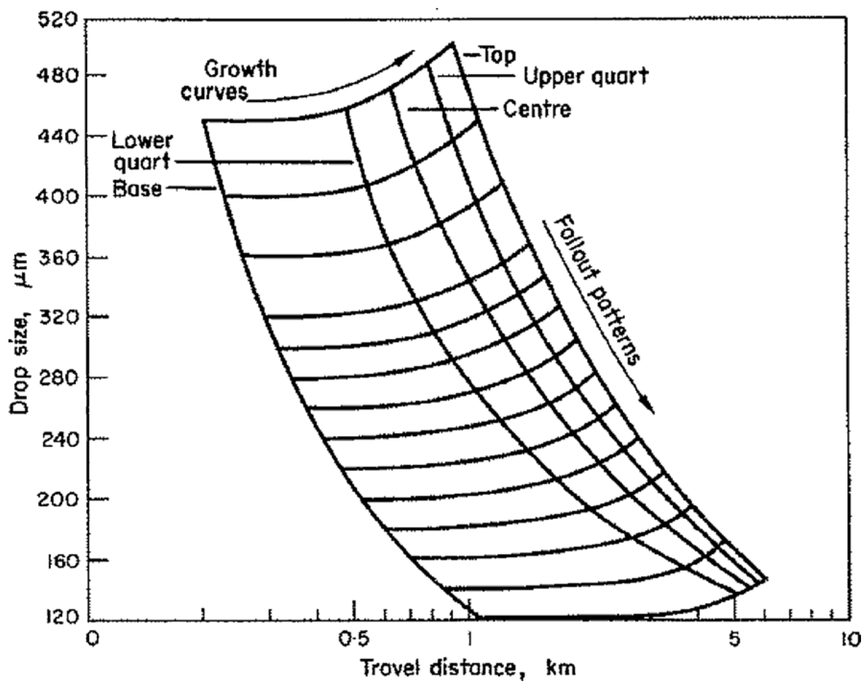


Fig. 3. Droplet growth curves and fallout patterns for different starting positions in plume.

Hong Kong, Europe, and Canada) in the air than can be held at equilibrium, the condensation occurs and a dense and persistent plume formed. On the other hand, during hot and dry weather conditions, the ambient air in the cooling tower may be heated and remixes along the lines 4–3, which is fully in the sub-saturated region and no plume is formed. As mentioned in above section, the exhaust of the tower is generally saturated and during odd whether conditions cannot be absorbed fully by the surrounding air, as a result, the access appears as visible fog. As shown in Fig. 2(a), the larger is the temperature difference between Inlet and outlet air of the tower, i.e. the greater the area of the intersection to the left of the saturation curve, Fig. 2(b), the more intense will be the plume. As the exhaust of the tower is almost saturated, the main parameter causing plume is the temperature difference between the inlet and outlet air of the tower. From Fig. 2(b) it can be seen that the intensity of plume is more for lower ambient temperature and less for higher ambient temperature. Thus by joining these two points by a straight line on the psychrometric chart, we can predict the possibility and potential of plume. So the potential of fog can be predicted by calculating the area of intersection as shown in Fig. 2(b).

Foster [25] worked on droplet growth inside and outside the cooling towers. In his study a simple model of a cooling tower plume has been used to estimate the precipitation and growth behavior of carryover droplets which rise within and then subsequently fall from the plume downwind of the cooling towers. In a 4 m/s wind speed using the excessively high carryover rate measured at Ratcliffe-on-soar power station, the calculated precipitation rates reached road wetting levels as far as 2.5 km downwind and nuisance levels up to about 4 km downwind. Droplets falling up to 1.5 km downwind had mass median sizes of approximately 300 μm, droplet sizes then got progressively smaller, being approximately 135 μm at 5 km downwind. For this reason only near field precipitation will persist in lower humidity conditions, far field precipitation being reduced to negligible levels by evaporation. Droplet growth curves and fallout patterns can be observed from Fig. 3 coalescence with the plume condensation droplets produced droplet (volume) growths of up to 40% for the larger droplets and up to 90% for the smaller droplets, besides these growths would have increased in the presence of fog droplets.

Slawson [26] observed and predicted the natural draft cooling tower plumes at paradise steam plant. In his study the observation of time-mean plumes from the natural-draft cooling towers at the Tennessee Valley Authority's Paradise Steam Plant taken during the winter of 1973 and has been compared with a one-dimensional model for moist plume behavior. The simple closed form integration model (CFIM) presented in the study simulates the observed visible plume behavior reasonably well. However, since the CFIM uses a constant wind speed over the plume rise region, it must be applied in a step wise manner over downwind distance and/or height above source in order to incorporate more accurately vertical variations in ambient temperature and relative humidity. Also, a constant wind speed biased to the final plume rise region was required by the CFIM in order to simulate the observed plume trajectories in a better way. The use of a numerical integration model (NIM) allows one to incorporate directly into the model the effects of vertical variations in ambient temperature, humidity and wind speed. In the reduction of the photographic data on the observed visible plumes it was found necessary to account for the observed changing plume direction with height above the source since, the use of a single average plume direction often led to significant errors associated with plume trajectory and length.

Dittenhoefe et al. [27] worked on number of airborne plume sampling experiments designed to examine the importance of sulfate particle-generating chemical reactions within coal-burning power station plumes. The flights were conducted downwind of the Keystone Generating Station in western Pennsylvania, with the Penn State University research aircraft, an aero commander 68OE. On-board aerosol sampling instrumentation included a condensation nucleus counter, an optical particle counter, and an electrical aerosol analyzer. A casella cascade impactor containing electron microscope copper grids coated with carbon film has been used to collect particles at varying distances from the stacks. These samples were analyzed for sulfate content and particle size distribution and the measurements of SO_2 were made with a rapid-response pulsed fluorescent analyzer. Atmospheric pressure, temperature, dew point, wind speed and aircraft position were also monitored. They [27] found that there exists more than one mechanism acting in the conversion of SO_2 to sulfate within power plant stack plumes.

Under the conditions of low relative humidity, near-neutral stability, and intense solar radiation, it was found that the production of new particles within the stack plume has been the dominant chemical process. It is likely that photochemical reactions involving SO_2 as a major source of these particles. Within a merged plume nearly 100% relative humidity, the net production of new particles was of relatively minor importance as compared with the growth of pre-existing droplets by absorption and oxidation of SO_2. Many of these droplets grew to the size of 0.3 pm and/or greater after 90 min of travel. They [27] also observed that, the highest rate of particle growth found to be average plume temperature was at its lowest (−16.8 °C) and least growth during the case of highest temperature (16.7 °C).

Köenig [28] studied on anomalous snowfall caused by natural-draft cooling towers. In his study, the field observations and numerical simulation has been used to define circumstances under which plumes from large natural draft cooling towers could be expected to glaciate and cause snowfall. According to his study the amount of snow falling from cooling tower plumes depends on the outcome of the competition between the evaporation of the plume and the total growth of ice particles. The evaporation of the plume depends on the ability of the ambient air to receive water vapor that is, the saturation deficit of the ambient air and the rate of mixing of the plume with its surrounding air. In ice supersaturated environments, the snow flux is not limited by evaporation but may be limited due to the fallout of snow particles and the inability of any mechanism to replenish them. Observations, theory, and numerical experiments all point to criteria of temperatures below −13 °C and ambient water vapor deficits less than 0.5 g/m^3, for a measurable snow to fall within about 50 km of a 1000 kg/s water vapor source, assuming the wind speed of the order of 10 m/s. The simulation, results strongly suggest that the closest deposition of snow as a function of the vertical rise rate of plume elements and their degree of mixing with the environment. Thus, the colder the plume the greater the concentration of ice particles and the greater the amount of snow created.

Spillane and Elsum [29] predicted the effects of cloud in plume of chimney. In this study a numerical model to predict the occurrence of visible condensation and cloud length of plumes in chimney has been tested against the observations of the plume from a 500 MW natural gas-fired power station at Melbourne, Australia. The criterion for a plume to be visible has been developed for droplets around 5 μm radius and distribution of plume and condensed water determined from Gaussian two dimensionlization of temperature and total water. The model correctly discriminates between cloudy and non-cloudy plumes and between persistent cloud that extends into the far field and occasions when cloud terminates within the coherent plume phase. On these latter occasions, the maximum cloud-extent predicted (MODEND) is the extreme sampled approximately 30 observations each 2 min apart. This extreme is highly correlated with other plume characteristics which also can be reliably obtained from the model prediction of extreme length. There is a potential to develop the model further to cover those cases where only wisp-puffs extend to the far field and the significantly dense cloud ends within the coherent plume phase. The results presented in their study [29] emphasized that good meteorological data are required for accurate theoretical prediction of plume behavior.

Spillane and Elsum [30] calculated the behavior of the plume from a wet cooling tower, in circumstances typical of strong boundary-layer convection, using an integral-plume model. Results suggests that, the fumigation of switch-yards by convective knock-down of cloudy plumes from large natural draft cooling towers in Australia, is considered so unlikely, it may be ignored against the more common effects of rain and fog, and possible "blow-out" by very strong winds. The centre line trajectories of cloudy and clear portions of the plumes, derived from the model for surface

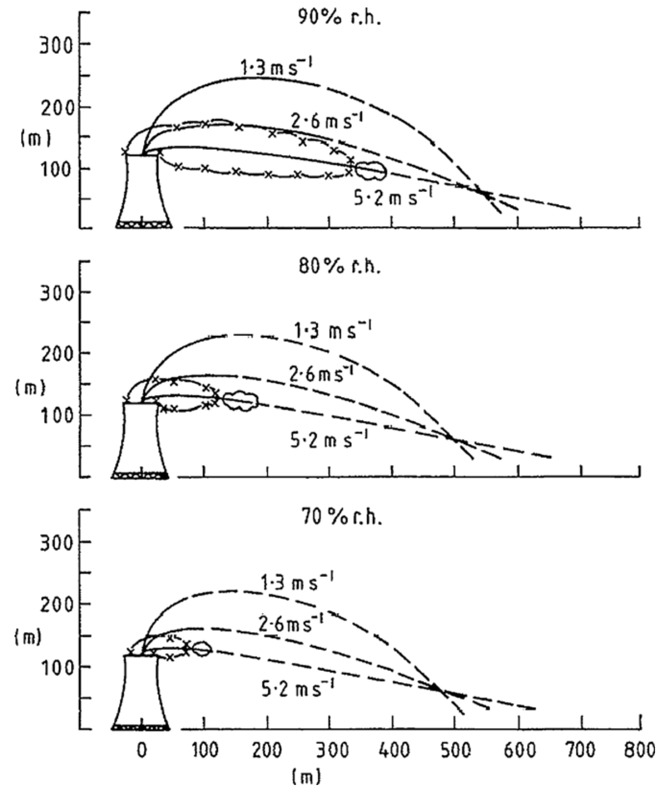


Fig. 4. Plume centre line trajectories for W_e, given by Eq. (1) and various horizontal wind speeds and environmental relative humidities (r.h.) —, cloudy; —-, clear; ∩ × ∩ condensation zone. (a) T_e = 15 °C and (b) T = 30 °C.

temperature of 15 and 30 °C, are given in Fig. 4(a) and (b). The 20 °C and 25 °C trajectories and cloudy portions lie within the ranges embraced in Fig. 4(a) and (b). While radii of zones of condensation have been calculated along each of the plumes they are shown only for the 5.2 m/s wind case and at 50 m intervals along the plume to avoid confusion in presentation. In these figures the radii are shown as crosses (x) and some licence is taken in pictorial presentation of the condensation zone. It is seen that the plume does not continue cloudy within 85 m of the ground for even the most adverse situation of, T_e = 30 °C, r.h. = 90%, U_e = 5.2 m/s as shown in Fig. 4(b). At higher wind speeds the entrainment of the lower cloudy parts of a plume into the turbulent wake of a tower has been discussed by Overcamp and Hoult [31] and Barber et al. [32]. As pointed out by Moore [33] very low temperatures (sub-freezing) are required for cloud-fog to extend to the ground in such turbulent wakes. The reduction in maximum rise of the plume as temperature increases from 15 to 30 °C is due to the reduction in flux of buoyancy from a natural draft cooling tower, as the ambient temperature rises, an increasing fraction of the waste heat is latent rather than sensible heat. The downdraft velocity profile given by Eq. (1) has been used with all combinations of temperature, humidity and horizontal wind speed to test the possibility of water droplet fumigation. It will be exceeded by less than 10% of downdrafts in a well mixed convective layer of about 1 km deep in days of strong heat flux (∼200 W/m^2).

$$W_e = \begin{cases} \dfrac{Z}{45\,(\text{m/s})}, & Z \leq 90\,\text{m} \\ 2\,(\text{m/s}), & Z < 90\,\text{m} \end{cases} \quad (1)$$

Campistron [34] studied the interaction between the natural snowfall and cooling tower plume. In this study a precipitation band, about 30 km long and 2 km wide, downwind of a nuclear power plant was observed with a millimetric Doppler radar. Huff

[35] postulated that a possible consequence of wet wastes from cooling towers could increase the natural snow precipitations falling in the wet plume through a seeder–feeder mechanism. The reality of such a phenomenon has now been experimentally demonstrated with the fine-scale three-dimensional observations of a Doppler radar. At the exit from the 0.6 km deep plume, the mean snow precipitation rate was approximately enhanced by a factor of two. This corresponds to an extraction rate of water in the plume by snow scavenging of 600 kg/s that is about one third of the water injection rate into the atmosphere by the cooling towers. They [34] has moreover showed that one of the results of this type of interaction is that snow precipitation can partly cleanse the plume and bring back to ground the condensed water which normally would have been dispersed in the atmosphere. In addition to these microphysical results, the Doppler capabilities were shown to be able to define the plume behavior by means of the dynamic perturbations caused by thermal effluents. The seeder feeder mechanism plays a major role in the initiation and growth of precipitation in extratropical systems which appear as a result of this study, that wet plumes can be, under certain conditions, unique laboratories for quantitative studies of such phenomena.

Schatzmann et al. [36] studied on flue gas discharge from cooling tower, wind tunnel investigation of building downwash effects on ground level concentrations. German power plants are required to meet new emission standards which limit the maximum sulfur dioxide (SO_2) concentration in flue gas discharges to 400 mg/m^3. To achieve this level of reduction in SO_2, concentration, wet scrubbing is necessary for large plants using lignite and/or hard coal. Wet scrubbing results in the significant reduction of the flue gas temperature leading to low effective stack heights. Instead of using stack gas reheating to achieve the necessary plume rise to satisfy local environmental standards, it was proposed to discharge the scrubbed flue gas from the existing natural-draft cooling towers (NDCT). For a 2700 MW lignite-fired power plant near Cologne/Country/province a wind tunnel study was carried out to investigate the effects of tower and building downwash effects on the ground-level concentrations of SO_2 produced by discharging the scrubbed flue gas from the natural-draft cooling towers. Also, a comparison was made between the ground-level concentrations produced by the cooling tower discharge method and those produced by a traditional stack. Results from the wind tunnel experiments described in this study contribute to the understanding of the downwash behavior of cooling tower plumes. The results also motivate a methodology for evaluating the ground-level concentrations due to Rue gas discharges from cooling towers, as required by the German Clean Air Act. The wind tunnel investigation proved, furthermore, that the release of scrubbed flue gas from natural-draft cooling towers into the atmosphere appears to provide an environmentally acceptable alternative approach to the conventional stack gas discharge. The time and expense required for such model experiments is considerable. However, general as well as site-specific results can be achieved which are unobtainable by any other means since the power plant units and/or specific plant buildings may not yet have been built. The alternative for existing plants under consideration for back fitting is more expensive field experiment.

Majumdar and Rodi [37] worked on three-dimensional computation of flow past cylindrical structures and model cooling towers. In this study they [34] presented a 3-D finite-volume method for calculating the flow and plume spreading past surface mounted cylindrical structures. It employs an orthogonal cylindrical-polar body-fitted numerical grid and the standard k–ε turbulence model with wall functions for bridging the viscous sub-layer. The application of the method to the flow around a circular cylinder and a cooling tower model showed that many of the very complex flow features in the vicinity of circular structures immersed in a boundary layer could be simulated realistically. These features include the formation of the horse-shoe vortex, the separation behind the structure in particular, the separation line on the cylinder, the separation on the roof, the formation of vertical and longitudinal vortex systems, the interaction of the bending-over jet in the case of the cooling tower model with the flow around the tower, and the general pressure distribution on the cylinder surface. The flow development near the ground was found to be very sensitive to the near-wall characteristics of the oncoming boundary layer and to the boundary conditions prescribed on the ground which determine the further development of the boundary layer.

Wei et al. [38] conducted study to clarify the mechanism of unfavorable effects of wind on the cooling efficiency of dry cooling towers full scale measurements. A hot water circulation system and fin-tubular radiators have been used for simulating the thermodynamic process of dry cooling towers. A dimensionless parameter, wind effect coefficient C_w, was defined and measured to describe the wind effects on the efficiency of cooling tower radiators. In this study they [38] found that: firstly in the regular wind speed region, the cooling efficiency of a dry cooling tower with a vertical radiator at the tower base is less than that when there is no wind at all. The curve of the wind effect coefficient (C_w) versus the wind velocity ratio (V_w/V_i) takes the approximate shape of an inverted parabola secondly winds lowers the efficiency of dry-cooling towers because of three reasons: (a) the wind forms an unfavorable pressure distribution at the tower inlet, (b) the wind breaks the hot plume rising from the cooling tower, and (c) the wind causes the back flow induced by the separation vortex at the leading edge of the tower outlet. Thirdly the leading-edge separation of the wind at the tower outlet will increase the tower draft. When this favorable effect is weaker than the sum of the total unfavorable effects mentioned above, the wind will lower the cooling efficiency of the dry cooling tower.

Derksen et al. [39] have studied the effects of wind speed on the air intake flow rate of a cooling tower: Wind tunnel study in three parts. In first part a wind tunnel model of a double-cell induced draft counter flow cooling tower has been tested to determine the effect of wind speed on the air flow rates entering the tower. This model differs from a typical building in that some flow passes through the model. The interaction of the flow with the cooling tower is documented as of the flow pattern in the vicinity of the tower. The study demonstrated that wind has a significant effect on the performance of cooling tower. At higher wind speeds, more flow enters the tower through the windward intake. For example, for a prototype wind speed of 8.9 m/s, the wind tunnel study suggests that the windward intake flow would increase by 45% and the leeward intake flow would decrease by 19%. This imbalance may be responsible for an increase in the accumulation of ice at the windward intake, since higher flow rates cause a greater local heat loss. Cross-sectional view of a counter flow cooling tower and scale model of a double-cell induced draft counter flow cooling tower is shown in Fig. 5.

Macdonald et al. [40] worked on water flume study of the enhancement of buoyant rise in pairs of merging plumes. When multiple stacks are grouped or ganged together at a site, the effluent plumes are often observed to merge downwind, forming a single buoyant plume whose rate of rise enhanced relative to the rise of the plumes individually. The magnitude of this rise enhancement depends on many factors, and the few available models for rise enhancement do not always agree with one another. In their [40] study the rise behavior of pairs of merging, buoyant plumes has been studied by the physical modeling in a water flume at 1:500 scales. The experiments have been conducted at several stack separation distances and various exit velocity ratios for stack pairs aligned with, and/or perpendicular to, the ambient flow. A list of the experimental test parameters for several of the stack

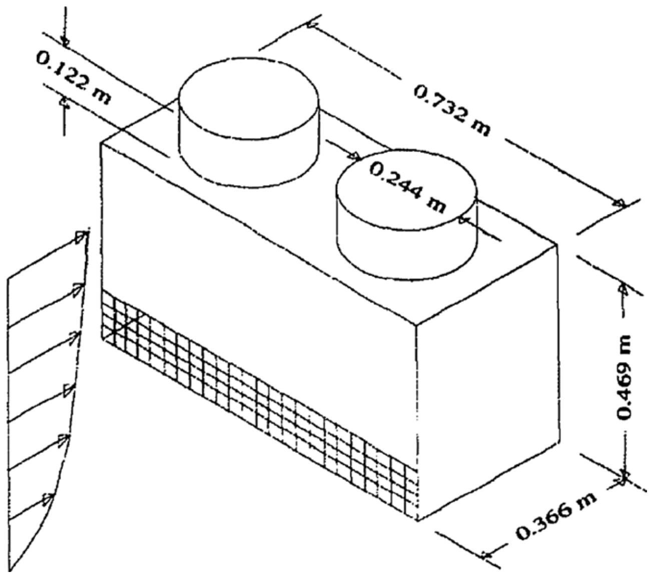


Fig. 5. Scale model of a double-cell induced draft counter flow cooling tower.

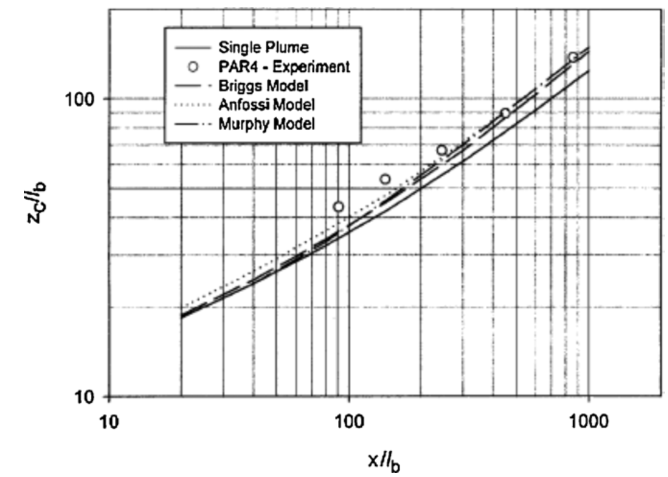


Fig. 6. Comparison of three plume rise models to the plume rise data from a pair of plumes parallel to the wind with exit velocity $w_s/U_H = 3.4$ and separated by $S/D = 6$ ($w_s/U_H = 3.4$).

configurations tested are given in Table 1. The experimental identifier refers to the stack configuration: S = single stack; PER = two stacks perpendicular to wind; PAR = two stacks parallel to wind; and, ANG = two stacks at an acute angle to the wind. Some experiments were also conducted with the stacks aligned at other angles to the flow. The stack releases were made buoyant by heating the source water, and the resulting plumes were measured with an array of sensitive temperature probes. From these measurements it was possible to determine the plume structure and the rise rates. Momentum shielding does not occur in the perpendicular stack configuration, so it is not surprising that the combined plume rise is found much lesser than the in such a case. In the empirical plume rise models for multiple sources presented by Briggs [41,42], Murphy [43], and Anfossi et al. [44], the plume rise enhancement factor is a function of only the stack spacing (S) and not of the stack angle to the flow. These models do not predict the current data at all well in the near field, probably because they were intended only to capture the effect of combined plume buoyancy which is active later in the trajectory. Fig. 6 shows a comparison of the measured plume rise data for the PAR4 configuration ($S/D = 6$) with these rise enhancement models. All the plume rise enhancement models seem to perform well at large fetch to predict the final rise height of the plume but they seriously underestimate the enhanced transitional plume rise. Based on the current data Anfossi et al. [44] model appears to be the best for predicting the near field behavior of merging plumes in the parallel configuration.

Table 1
Single and paired stack test parameters.

Experiment identifier	Stack angel (deg.)	S/D	w_s/U_H
S1, S2, S3	N/A	N/A	1.7, 3.4, 6.8
PER1, PER2, PER3	90	3	1.7, 3.4, 6.8
PER4	90	6	3.4
PER5, PER6, PER7	90	9	1.7, 3.4, 6.8
PAR1, PAR2, PAR3	0	3	1.7, 3.4, 6.8
PAR4	0	6	3.4
PAR5, PAR6, PAR7	0	9	1.7, 3.4, 6.8
PAR8	0	18	3.4
ANG1	18	9.5	3.4
ANG2	33	10.8	3.4

Tyagi et al. [45] presented a case study of the prediction, potential and control of plume in wet cooling towers from a huge commercial building in Hong Kong based on the weather data available for a particular year. In their study, the concerned building is one of the tallest in the world with the central air conditioning system containing six water-cooled chillers and 10 cooling towers. A simple line diagram of a chiller coupled with a building envelope (space to be cooled) and a cooling tower (to extract heat from the condenser of the chiller) and a heat pump (to heat the exhaust of the tower) is shown in Fig. 7 (a) and formation and potential of plume is shown in Figs. 7(b) and (c). They [45] predicted that, the power input is found to be lower and the coefficient of performance (COP) moderate when all the 10 towers with low speed are in use, while it is found to be reverse when there are five towers, especially, three low and two high-speed towers are used. It is also found that the combined heating and cooling option can be a better approach than that of the heating option alone from the point of view of thermodynamics as well as from the point of view of economics. The COP of the chillers increases from 6.01 to 7.09 when the number of cooling towers increases from five to ten. On the other hand, the power consumption first decreases and then increases which is mainly due to the increment in the consumption of fan power from 270 to 900 kW for both options. The overall power consumption decreases slightly for the combined heating and cooling option, while in the heating option, the overall power consumption increases slightly. However, it is observed that a proper operation of cooling towers is an effective means to control and/or at least reduce the potential of visible plume generated by wet cooling towers at the existing chilling plant design for this particular building.

Wang et al. [46] presented a comparative case study on the application and utility of solar collectors heating system to control the visible plume from wet cooling towers of a huge commercial building in Hong Kong. They [46] argued that, since the solar energy is free of cost and can be utilized provided advance technology could be used but at the same time it is intermittent in nature, and sometime there may be no more sun light due to raining and/or clouding weather. In such a situation, solar collector alone cannot be the ideal solution, unless there is some alternative to assist such system. They also presented few fruitful discussions, such as, large temperature difference in the inlet and outlet temperature of collector fluid, either the number of collectors and/or the mass flow rate of the fluid should be higher while it could be reversed in the case of smaller temperature difference. Also since the temperature of the refrigerant is much higher at the exit of the compressor, i.e.

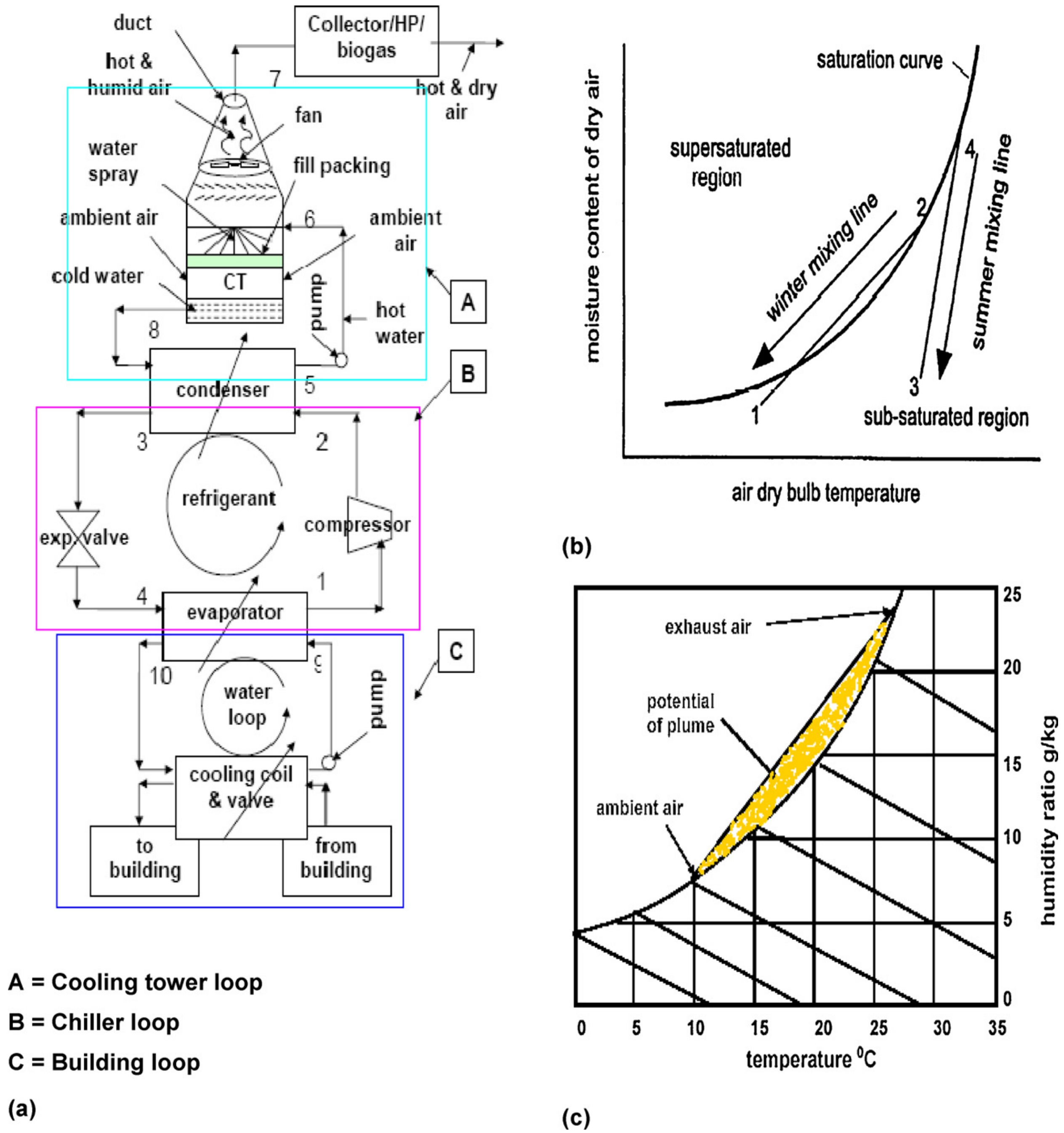


Fig. 7. Line diagrams of: (a) the proposed system; (b) the formation of plume (fog) in a wet cooling tower; and (c) the potential of plume in a typical cooling tower. (a) A, cooling tower loop; B, chiller loop; C, building loop.

at the entering of the condenser. So a desuperheater may be used to heat the exhaust of the cooling towers which not only could save energy but also could reduce the load of the cooling tower and hence, the overall building load. Another way to solve this problem is that one or two chiller could be air cooled and the heat air could be mixed with the exhaust of the cooling tower before being released into the atmosphere.

Gao et al. [47] experimentally studied the heat transfer performance of the natural draft counter-flow wet cooling for cases with cross-wind conditions, the schematic diagram of experimental cooling tower and sketch map of water-air flow within the cooling tower are shown in Figs. 8 and 9 respectively. The variation of circulating-water temperature difference (ΔT) and the cooling coefficient of efficiency (η) with cross-wind velocity, circulating water inlet temperature and flow rate, had been shown under cross-wind conditions, compared with cases without wind. According to experimental results, it is found that, under the same ambient meteorological parameter and windless conditions, both circulating water temperature difference and coefficient of efficiency increase with rising the circulating water inlet temperature, decrease with rising water flow rate. The cross-wind has a great influence on the circulating water temperature difference and coefficient of efficiency, and it can make them decrease by about 6% and 5%, respectively. There is a critical value during the variation of circulating water temperature difference and coefficient of efficiency with wind velocity. While the critical Fr_l number which is received from the critical wind velocity is not more than 0.174, the temperature difference and coefficient of efficiency reduce with rising

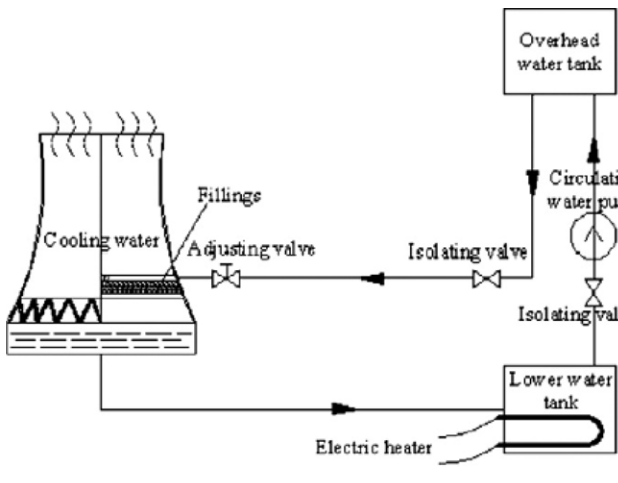


Fig. 8. Schematic diagram of experimental cooling tower.

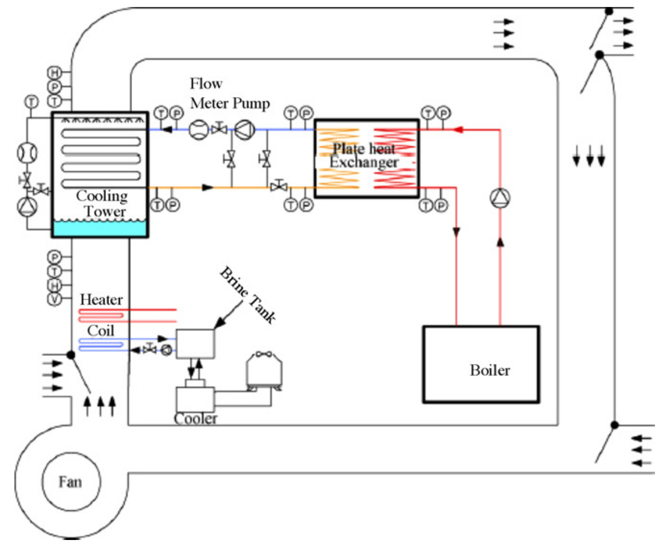


Fig. 10. Schematic of the experimental apparatus.

the wind velocity, and while this critical Fr_l number is more than 0.174, both of them increase with the increment of wind velocity. In this paper, many correlative equations are received, including windless conditions and cross-wind conditions, and the errors of all of the equations are in the tolerance, so they may be applied into engineering practice.

Tyagi et al. [48] presented a case study based on the economic considerations and comparisons between the heat pump and solar collector heating systems for the application and utility to control the visible plume from wet cooling towers of a huge commercial building in Hong Kong. A detailed economic study for both cases, i.e. for heat pumps as well as for solar collectors had been done and compared using different (capital and operational) costs, taking other constraints into account. They found that, the air-cooled systems are found to be more expensive than those of water-cooled systems. It can be seen from different tables (Tables 2 and 3) that almost every cost (investment, running, maintenance, and power input) in the case of air-cooled heat pump system is found to be much higher than those of the water-cooled heat pump system. The results about the costs and use of the electric and the geothermal heat pump systems indicate that the investment cost and other cost of an electric heat pump (EHP) system is lesser than the geothermal heat pump (GHP) system while it is reverse in the case of the running cost. For solar collector system, the fuel (the sun light) is free and the investment cost is very less as compared to those of the heat pump systems and hence, the former is much cheaper than the latter. Again, the running cost for the solar collector systems is nominal as compared to those of different heat pump systems and can be a better option from the point of view of economics as well as from the point of view of thermodynamics. So the application of solar collectors can be an alternative but may not be a substitute provided weather condition is not a big constraint. Finally they found in their study that, the combined heating and cooling option is feasible only in the case of heat pump systems and hence, the solar collector cannot be used for dual application. The combined option not only consumes less energy but also utilizes the cooling produced by the heat pump system and hence, the combined option is more economical than the heating alone option especially in the case of heat pump systems.

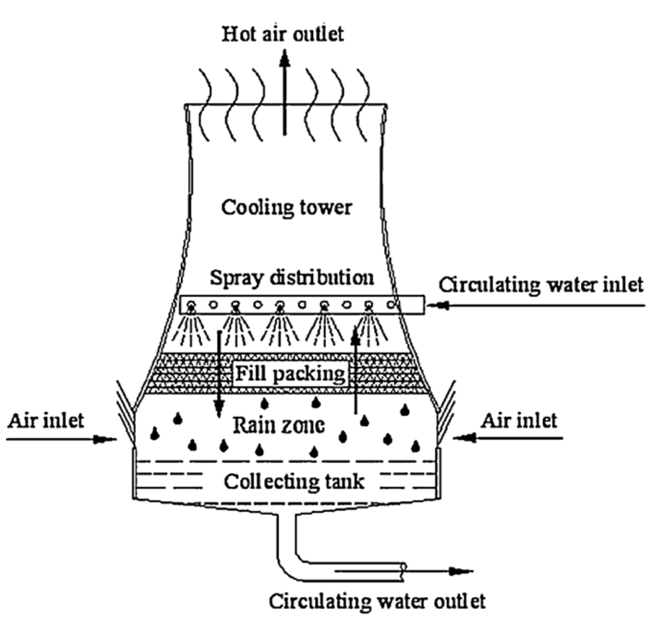


Fig. 9. Sketch map of water–air flow within cooling tower.

Xu et al. [49] worked on the evaluation of the plume potential and its effect on the sizing of the plume abatement system in a large commercial office building in Hong Kong for practical application. The evaluation has been conducted based on a dynamic simulation platform using the typical meteorological condition of Hong Kong. Dynamic simulation of the cooling tower and chiller systems of a high-rising building using the typical meteorological data of Hong Kong showed that the low temperature is not reliable to be used as a design point of the plume abatement in subtropics. Besides, the yearly dynamic simulation is essentially important to predict the plume potential and determine the parameters for the system design of the plume abatement. The results also showed that alternative control strategies have significant impacts on the frequency of the occurrence of the plume and the maximum heating requirement for the plume abatement. Therefore, the set-point control logics of the supply cooling water temperature and fan modulation methods should be seriously involved in for the design of the plume abatement system.

Sarker et al. [50] have done an experimental study (as can be seen in Figs. 10 and 11) on performance characteristics of the hybrid closed circuit cooling tower (HCCCT) having a rated capacity of 136 kW. Bare-type copper coil having an outer diameter of 15.88 mm has been used in the 1.14 m × 2.36 m × 3.2 m dimensional tower. Cooling capacity and pressure drop have been studied with respect to variable air inlet velocity, wet-bulb temperature,

Table 2
comparison between costs and power consumptions for water and air cooled heat pump systems.

Heating capacity (kW)	Consumption of power (kW)				Different costs (in US$)					
	Heat pump		Chiller	Fans[a]	Capital		Running		Other	
	Water	Air			Water	Air	Water	Air	Water	Air
1988.8	390.0	641.5	3486.5	270	119,807	215,653	520	855	5990	10,783
1311.2	257.1	423.0	2651.4	450	78,988	142,178	343	564	3949	7109
963.6	188.9	310.8	2834.1	270	58,048	104,487	252	414	2902	5224
917.7	179.9	296.0	2633.7	300	55,283	99,510	240	395	2764	4975
786.6	154.2	253.7	2651.4	450	47,386	85,294	206	338	2369	4265
655.5	128.5	211.5	2462.7	600	39,488	71,078	171	282	1974	3554
563.7	110.5	181.8	2404.2	900	33,958	61,124	147	242	1698	3056
491.7	96.4	158.6	2462.7	600	29,620	53,317	128	211	1481	2666

[a] Fan power consumption depends on the speed and number of cooling towers in use.

Table 3
Comparison among various costs between electric and geothermal heat pump systems.

Heating capacity (kW)	Investment cost (US$)				Operational cost (US$)							
					Running cost[a]				Other cost[b]			
	EHP		GHP		EHP		GHP		EHP		GHP	
	Water	Air	Water	Air	Air	Water	Air	Water	Water	Air	Water	Air
1988.8	413,017	442,519	531,022	590,025	688	597	533	394	12,391	13,276	15,931	17,701
1311.2	272,299	291,749	350,099	388,999	453	394	352	260	8169	8752	10,503	11,670
963.6	200,112	214,406	257,287	285,875	333	289	258	191	6003	6432	7719	8576
917.7	190,580	204,193	245,032	272,258	317	275	246	182	5717	6126	7351	8168
786.6	163,355	175,023	210,027	233,364	272	236	211	156	4901	5251	6301	7001
655.5	136,129	145,852	175,023	194,470	226	197	176	130	4084	4376	5251	5834
563.7	117,065	125,426	150,512	167,235	195	169	151	112	3512	3763	4515	5017
491.7	102,112	109,406	131,287	145,875	170	148	132	98	3063	3282	3939	4376

[a] Running cost is calculated for per day.
[b] Other cost is considered to be 3–5% (annually) of the capital cost.

cooling water inlet temperature and air to cooling water volume flow rate ratio (G/W). The lower performance of the cooling tower was found in the dry mode operation of HCCCT, which was cost-effective due to the lower power consumption. In wet mode, wet-bulb temperature at the experimental condition was found to be 27 °C and the cooling capacity at this variable wet bulb temperature (WBT) was 130.5 kW, which is about 4% lower than the rated capacity. The capacity in this regard to the cooling water inlet temperature was 134.7 kW which agreed well with the rated capacity. Very similar capacity was noted with respect to the ratio of air to the cooling water volume flow rate. The pressure drops in wet mode operation were seen to increase almost exponentially with the increase of the air velocity and the pressure drop was about 39.3 Pa for the wet mode. The result obtained from this study is supposed to provide basic relevant data that could be referred for the optimum design of the hybrid closed circuit cooling towers.



Fig. 11. Photograph of the experimental apparatus.

Wang et al. [51] studied the evaluation of alternative arrangements of a heat pump system for plume abatement in a large-scale chiller plant in a subtropical region. According to them heat pumps could be used to produce hot water for hybrid cooling towers for preventing the occurrence of plume in subtropical regions. The evaporative side of the heat pump system could be arranged either at the inlet side or at the outlet side of these cooling towers for cooling down the cooling water temperature. Alternatively, the evaporative side of the heat pump system could also be arranged at the evaporative side of chillers to reduce return chilled water temperature and therefore to reduce the cooling load of chillers. This study presents the evaluation of the impacts of these three arrangements (as shown in Figs. 12 and 13) of the heat pump system on the plume control performance and the energy performance in a large-scale chiller plant in Hong Kong. The analysis on the fogging curve for plume control based on the weather condition and the cooling load conditions of the chiller plant shows that this curve is reasonable for plume control in this chiller plant although it is slightly conservative which can be seen in Fig. 14. The simulation results show that different alternative arrangements of the heat pump system for plume abatement have sufficient plume control capability and similar plume control performance when the cooling water or the chilled water is used as the heat source of the heat pump system. Concerning the energy consumption aspect, results show that the arrangement of the evaporative side of the heat pump system either at the inlet side or the outlet side of cooling towers almost does not affect the energy performance of the chiller plant, and this impact could be ignored almost. However, when the return chilled water was used as the heat source of the heat pumps, the

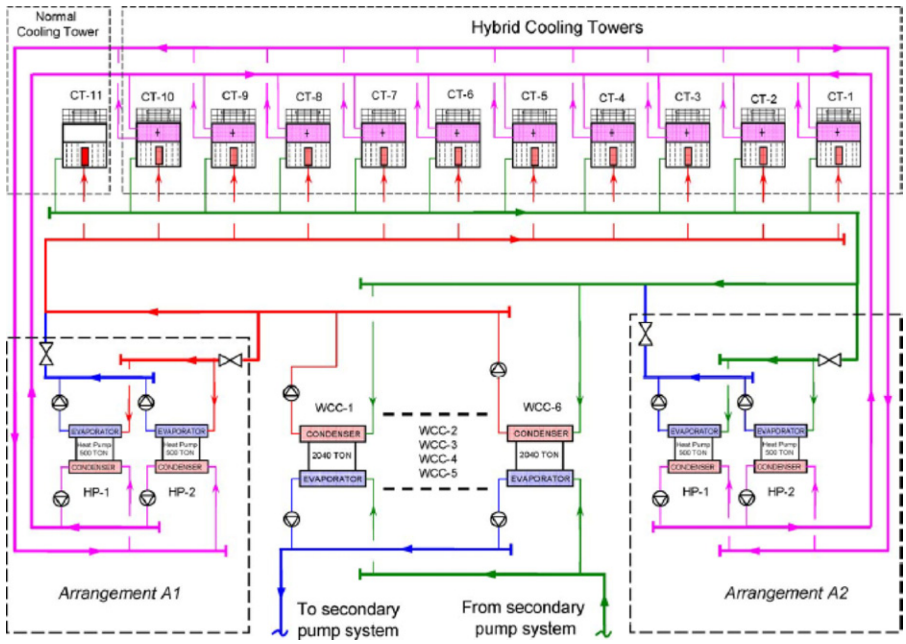


Fig. 12. Schematics of the chiller plant and the plume abatement system with alternative arrangements of the heat pump system (arrangement A1 and arrangement A2).

total energy consumption of chillers could be reduced up to 0.85%. This is mainly due to the cooling energy of the heat pump system is added in chilled water for reducing the cooling load of chillers directly. In this case, the power consumption of the heat pump system increased noticeably due to the low temperature of the heat source, therefore the lower is the COP of the heat pump. However, the reduction in chiller power consumption is significantly larger than the increase in heat pump power consumption. Utilization of chilled water as the heat source of the heat pump system for plume control is more preferable for improving the overall energy efficiency than utilization of cooling water as the heat source.

Lucas et al. [52] had worked on the influence of psychometric ambient conditions on cooling tower drift deposition, as water drift emitted from cooling towers is objectionable for several reasons, mainly due to human health hazards. A numerical model to study the influence of psychometric ambient conditions on cooling tower drift deposition was developed as a tool to evaluate liquid droplet dispersion and risk area. Both experimental plume performance and drift deposition were employed to validate the numerical results. The objectives of this work were threefold: the first one was to develop a computational fluid dynamics model to predict water droplet dispersion and surface drift deposition from cooling towers. The second one was to validate the model by using experimental data from literature. The third objective was to assess the influence of psychrometric ambient conditions such as dry bulb temperature and absolute humidity and water droplet exit temperature on drift deposition as well as on the size of the area affected by the cooling tower. The mathematical model presented, consisting of two coupled sets of conservation equations for the continuous and discrete phases, was incorporated in the general-purpose

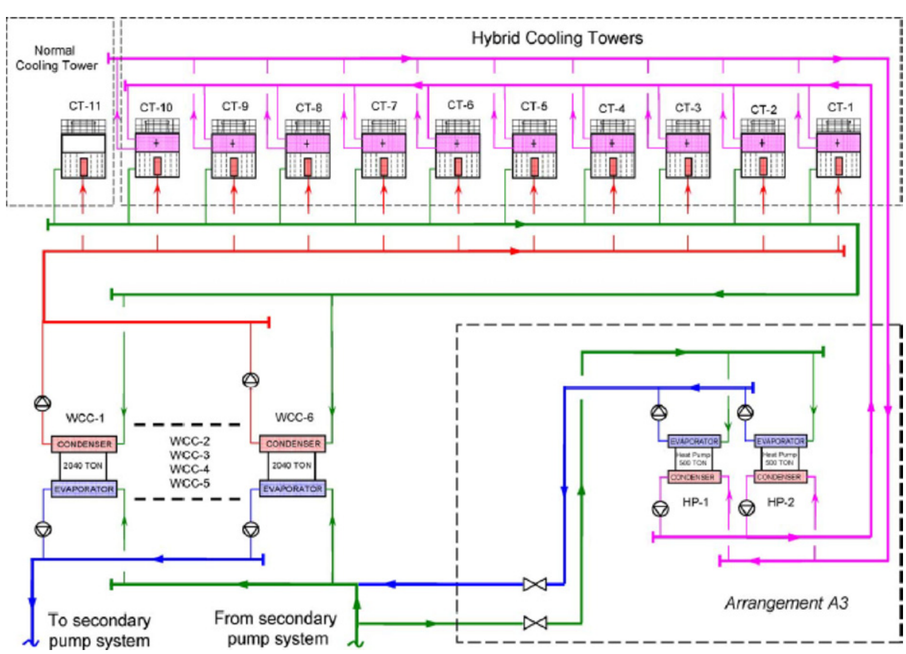


Fig. 13. Schematics of the chiller plant and the plume abatement system with an alternative arrangement of the heat pump system (arrangement A3).

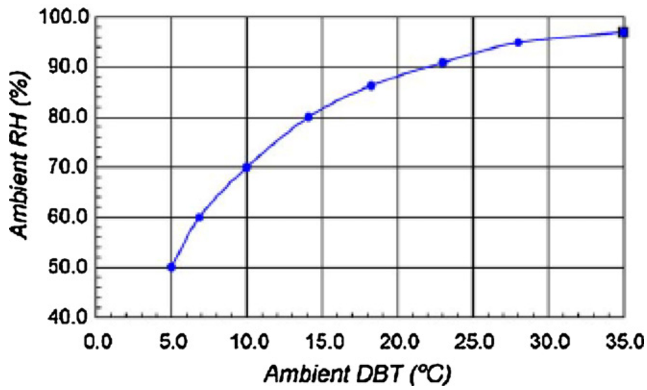


Fig. 14. The fogging curve for plume control.

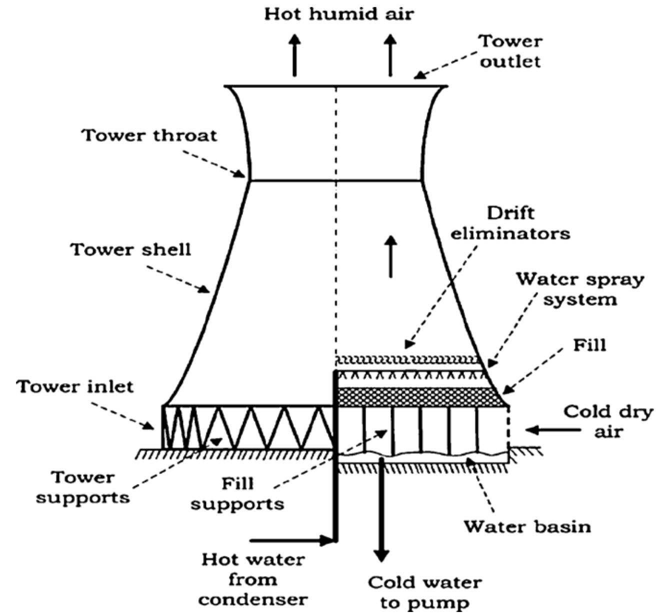


Fig. 15. Counter flow natural draft wet cooling tower.

computational fluid dynamics (CFD) code Fluent to simulate drift evaporation and deposition. Experimental results from Policastro [53,54] were employed to validate the numerical results in terms of plume performance and drift deposition. A good agreement was also obtained with the results provided by a previous numerical model developed by Meroney [55] for the same experiment (Chalk Point Dye Tracer Experiment). Although Meroney's model [55] did not take into account evaporation, the experiment was carried out in conditions of high relative humidity, which explains the lack of divergence between the results of both models. Once it was validated, the model developed by him showed the strong influence of ambient temperature on the cooling tower drift deposition and dispersion. For a higher ambient temperature, ground deposition found to be lower as also the case for the zone affected by the cooling tower. The effect of the other magnitudes/parameters included in the study are the ambient absolute humidity and droplet output temperature on the cooling tower drift deposition and dispersion found to be weaker than the ambient temperature. A high level of ambient absolute humidity increased ground water deposition and also the radius of the drift dispersion area. Regarding the last variable, a high level of droplet output temperature decreased ground water deposition but increased the size of the zone affected by the cooling tower due to the fact that droplets with a higher temperature at the tower exit arrived at the wet bulb temperature with a smaller size, which made them travel further.

Al-Waked [56] investigated the effects of crosswinds on the thermal performance of natural draft wet cooling towers (NDWCTs). A three-dimensional CFD model had been used to determine the effect of crosswinds on NDWCTs performance surrounded by power plant building structures. This model also utilized the standard k–ε turbulence model as the turbulence closure. Two cases had been investigated: a stand-alone NDWCT and two NDWCTs within a proposed power plant structures (PPS). Total eight crosswinds directions ($Q_{cw} = 0°, 45°, 90°, 135°, 180°, 225°, 270°$ and $315°$) with crosswinds speeds ranging from 0 to 15 m/s were investigated. It has been found that regardless of the crosswinds direction, an increase of 1.3k or more could be predicted at crosswinds speeds greater than 4 m/s. Furthermore, the performance of NDWCTs under crosswinds has been found to be dependent on the three major factors viz. the structure of the approaching crosswinds and whether it is disturbed or undisturbed, the location of the NDWCT in the wake of the other NDWCT, and the location of the NDWCT in front of/in the wake of the PPS. When comparing results from the stand-alone and from the NDWCTs within PPS simulations, differences in ΔT_{wo} were found to be less than 1 K for the whole span of crosswinds speeds and could be decreased to 0.7 K for speeds less than 8 m/s. Finally, results obtained from the simulation of a stand-alone NDWCT could be used instead of those from NDWCTs within PPS at a certain crosswinds direction for qualitative comparisons. View of natural draft cooling tower is given in Fig. 15.

3. Mathematical modeling and simulation

The development of the cooling tower analysis began in 1922, with the first work due to Robinson [2], who established the general principle applicable to cooling tower design and derived equations to be used by the designers, Robinson was the first to use Lewis work [1], who stated a series of fundamental concepts about the mechanism involved in the transfer of heat between liquid and gases and in the vaporization of liquids. Merkel [3] used the enthalpy potential as a driving force for air–water exchange and assumed a similarity between heat and mass convective transfers by stating the Lewis number equals one. His analysis and simplification have been used today. More recently, several authors have studied the convection phenomenon occurring in cooling towers. Baker and Shrylock [4] developed a detailed explanation of the concept of cooling tower performance, clarifying the assumptions and approximations used by Merkel. Shelton and Weber [8] used mathematical models based on manufacturer's performance data in order to investigate the effect of (low) water and air floe rates. Bernier [10] presented an analysis of basic heat and mass transfer processes occurring around a droplet in transient cooling. Mathematical modeling and simulation is divided into three parts as given below:

3.1. Modeling for visible plume

Chen Norbert and Jung [57] presented a mathematical model and computer programming of drift deposition to describe a bifurcated cooling tower plume. In this study cooling tower drift deposition modeling had been extended by including the centrifugal force induced by plume bifurcation as a mechanism for droplet removal from the plume. Bifurcation occurs in plumes that are bent-over either by a wind or by a temperature inversion. The bifurcated plume consists of two-line vortices of equal strength but opposite sense of rotation. The centrifugal force induced by the vortex motion in a bifurcated plume provides an additional mechanism for expelling drift droplets from a plume; previously considered droplet removal mechanisms are gravitational force

and turbulent diffusion. Although there is ample observational evidence for the existence of bifurcated plumes, the effects of the centrifugal force on the ground deposition patterns of cooling tower drift have received no attention. This study is thus the first systematic description of such effects. Specifically, this mathematical study is aimed to simulate a bifurcated plume and use this model to determine both the importance of the centrifugal force on drift droplet removal and a more realistic breakaway point. In the proposed model, the presence of the droplets is assumed not to affect the plume dynamics. Furthermore, the droplet is assumed to be in thermal equilibrium with the local environment for its entire lifetime, i.e. from the emission to impact. Thus, the energy transport between a droplet and its surroundings can be ignored. The model assumes that each separate arm of bifurcated plume rises as a single plume obeying a 2/3 law relation between rise and downwind distaste from the tower, grows as a cone following the empirical entrainment relation $dR/dz = 0.5$ in the bent-over rising stage, and rotates as o tube according to a free vortex law. When a plume is bifurcated, the model predicts that a droplet will follow a helical trajectory. The shapes of the trajectory depend on droplet size, vortex strength, point of emission, drag coefficient, and ambient conditions. When the ambient wind and droplet evaporation are ignored and the droplet is embedded in an unbounded vortex field, the model predicts that: (i) the smaller the droplet, the closer the droplet follows the vortex motions; (ii) the larger the drag coefficient, the longer the droplet is retained inside the plume; and (iii) for a heavier droplet in a weak vortex, the force of gravity dominates the centrifugal force. When the ambient wind and droplet evaporation are included and the droplet is embedded in a bounded vortex field, the model predicts a helical trajectory. The model is specifically designed for a single droplet; however, it can be generalized to compute the ground deposition rate if the distribution of droplet size at the tower mouth is available.

Golay [58] worked on numerical modeling of buoyant plumes in turbulent, stratified atmosphere. They [58] presented a model for bent-over plumes in atmospheres having complicated vertical structure. They used a mixed Eulerian–Lagrangian or parabolic modeling treatment in which a computational mesh oriented vertically and crosswind translates downwind at the local wind speed. Knowledge of atmospheric vertical profiles of wind speed, virtual potential temperature, relative humidity, turbulence kinetic energy and turbulent viscosity are required in a problem specification. A widely applicable model of buoyant bent-over plumes calculation had been developed. The advantage of the model is its ability to treat problems outside the scope of existing plume models without greatly increasing the resources required for the analyses. The validation of the model, however, must begin with a demonstration of its ability to reproduce the solutions to problems that are known to be solvable. This demonstration has proceeded along two lines in this work – problems in which the plume properties dominate the flow, and problems in which the atmospheric turbulent mixing dominates the flow. Some overlap between these simple regimes occurs, but in general the organization serves to highlight the cause of the particular successes and discrepancies in the model validation work. The results obtained from this model are found to be in good agreement with the laboratory results obtained in the plume dominated regime. The buoyant line-vortex motions and the Brunt–Vaisala period of a buoyant cylinder of fluid have been studied, and they compared favorably with the predictions. As a test of the integral hydrodynamic model, the Brunt–Vaisala, the period of the oscillation of a parcel of fluid perturbed from its equilibrium level in a stably stratified fluid. The formula given by Csanady [59] is given by:

$$\text{Brunt–Vaisala period} = \frac{2\pi}{\sqrt{g\, d\theta/T\, dz}}\,(\text{s}) \tag{2}$$

For typical atmospheric values of T and $d\theta/dz$, the period is of the order of hundreds of seconds. However, the unsuccessful attempts to "tune" the turbulence model coefficients point out the limiting assumption contained in the turbulence model used, particularly with regard to the buoyant production and anisotropy of turbulence. According to this study the predictions of plume rise and spreading in neutral atmospheres agree reasonably well with laboratory and field data, although some turbulence modeling limitations are evident in the comparisons.

Overcamp and Kut [60] introduced a virtual origin correction for bent-over jets and bent-over plumes by extrapolating the jet or plume to a point using the appropriate far-field rise law. This point is assumed to be the origin or source of the jet or plume. This correction was tested with four sets of data from model studies and one set of pilot-scale field data. The principal effect of the correction of the data is the change in the empirical coefficients C_m and C_b or the corresponding entrainment coefficients β_m and β_b for the one-third and two-thirds law, respectively. The far-field rise of a buoyant plume is described by the two-thirds law:

$$\frac{z}{l_b} = \left(\frac{3}{2\beta_b^2}\right)^{1/3}\left(\frac{x}{l_b}\right)^{2/3} \tag{3}$$

where β_b is the entrainment coefficient for bent-over plumes and l_b, is the buoyancy scaling length defined as

$$l_b = \frac{F}{u^3} \tag{4}$$

The two-thirds law is derived on the assumption that the plume emanates from a point source with buoyancy flux equal to the actual plume. The two-thirds law can be written as

$$\frac{z}{l_b} = C_b\left(\frac{x}{l_b}\right)^{2/3} \tag{5}$$

The rise of a bent-over jet is given by the one-third law:

$$\frac{z}{l_m} = \left(\frac{3}{\beta_m^2}\right)^{1/3}\left(\frac{x}{l_m}\right)^{1/3} \tag{6}$$

in which z is the rise above the stack, x is the distance downwind, β_m is the entrainment coefficient for bent-over jets, and l_m is the momentum scaling length defined as

$$l_m = \left(\frac{\rho_s}{\rho_a}\right)^{1/2}\left(\frac{w_o b_i}{u}\right) \tag{7}$$

in which ρ_s and ρ_a are the initial stack gas and ambient air densities, respectively, w_o is the efflux velocity, u is the mean wind speed, and b_i is the initial stack radius. The one-third law is derived on the assumption that the jet emanates from a point source with momentum flux equal to that of the actual jet. Equation can be written as:

$$\frac{z}{l_m} = C_m\left(\frac{x}{l_m}\right)^{1/3} \tag{8}$$

For the corrected data, the average value of C_m is 2.01 for Slawson and Rennie's [61] data and 2.07 for Wright's [62,63] data. This corresponds to entrainment coefficients of 0.61 and 0.58, respectively. With the correction, little if any dependence of these coefficients on speed ratio was seen for values of R between 3 and 20. The dependence reported by earlier investigators appears to be largely an artifact resulting from the neglect of the finite size of the stack. We tentatively conclude thaw β_m is approximately 0.6 with a corresponding value of C_m of 2.03 for R between 3 and 20. Further experiments should be conducted to determine the value of β_m with greater precision and to determine if it is a weak function of the speed ratio. For bent-over plumes, the corrected values of C_b

for all data except that of Fan ranged from 1.58 to 1.67 which corresponds to β_b ranging from 0.61 to 0.57. These values are in good agreement with the commonly accepted value of 0.6. The uncorrected values of C_b ranged from 1.4 to 1.54 which corresponds to β_b ranging from 0.74 to 0.64. Finally, comment on application of the virtual origin correction to model studies was given. If the stack height is geometrically scaled to the rest of the model but the stack diameter is exaggerated, there may be an artificial decrease in the plume rise approximately equal to the reciprocal of the entrainment coefficient times the difference between the actual mode stack radius and the radius of a geometrically scaled stack. This decrease might be compensated by a corresponding increase in the height of the model stack as suggested by Poreh and Kacherginsky [64]. This requires further testing prior to application.

Davidson [65] had worked on simultaneous trajectory and dilution predictions from a simple integral plume model. Studies of visible plumes from natural draft cooling towers have shown that, while simple integral plume models in the literature can be tuned to data to yield good predictions of a single variable such as trajectory, there is an underlying weakness in many of these models which becomes apparent when simultaneous predictions of more than one quantity are required. More complex integral models do not appear to have the same difficulty. By comparing the equations on which simple and complex integral models are based, he [65] concluded that the neglect of a dynamic pressure force in the momentum balance and in the formulation of the initial conditions for the simple model is the source of the problem. It had been shown that the addition of a dynamic pressure force to the vertical momentum balance, either through an added mass factor or through a conventional drag force, introduces a correction into the trajectory prediction for a buoyant plume, while leaving the form of the dilution prediction unchanged. The net effect is to allow trajectory predictions for a buoyant point source to be matched to measurements with a reduced value of the entrainment constant, thus bringing corresponding dilution predictions more into line with measurements. It is interesting that, although the added mass factor and a conventional drag term appear in different ways in the momentum balance, they appear in a formally identical way in the actual trajectory solution. The dynamic pressure correction to the momentum equation does not improve the performance of the simple model for a momentum source. It is shown, however, that a similar correction can be derived for momentum sources through a derivation of the initial condition for momentum flux consistent with the conservation equations used in the integral analysis.

Becker et al. [66] presented a method of numerically modeling cooling tower plume recirculation. As recirculation is directly related to the degradation of cooling tower performance. It is a measure of the ratio of the amount of exhaust air which reenters the tower divided by the total amount of air going through the tower. Assuming this exhaust air can absorb no energy from the hot circulating water, the effective size of the tower is reduced. The results of the current model show that in the 4 m/s case, the cooling capacity of the tower is 97.2% of its capacity with no recirculation; and in the 6 m/s case it is 97.9%. Thus, recirculation can have a significant effect upon tower performance and should be considered in the design of the tower.

Johnston and Wilson [67] proposed a model that uses a stream wise vortex pair embedded in the plume to produce a downwash velocity that varies with downwind distance and competes with the trajectory centerline plume rise velocity. The vortex-pair model proposed in the study provides a physical basis for understanding the process of down-wash. Even with their simplifying assumptions of an infinitely long pair of vortex lines gradually changing their spacing to produce an x-dependent downwash velocity, the model gives good estimates for the distributed effect of downwash on deflecting plume trajectories below stack height for weak jets. However, the model has a multitude of approximations hidden in the dependence of the vortex circulation parameter B_3 on jet strength M. The downwash component in equation given below:

$$h_m = \left[\frac{3M^2x}{4\beta^2 D}\right]^{1/3} - B_3\left[\frac{x}{D}\right]^{0.6} \tag{9}$$

where β and B_3 are empirical constants that depend on the density-weighted velocity ratio M, D is inside diameter should be used with caution beyond the limit of $x > 300$ where the experimental measurements ended. With the exception of Snyder and Lawson [68], all laboratory experiments have been limited to sub-critical Reynolds numbers where the boundary layer on the cylindrical stack model is laminar at the point of separation and vortex rollup. Their experiments were no exception, with a very low external Reynolds number of 1800, and were in good agreement with the subcritical measurements of Snyder and Lawson [68]. Because virtually all full-scale stacks are in the supercritical regime with a turbulent boundary layer at the point of flow separation from the cylinder, more experiments are needed at these supercritical conditions to determine if a vortex-pair model is appropriate for predicting downwash for full-scale stacks. In addition, there is a need for experiments on buoyant jets to determine if the vortex-pair model is viable for combined momentum and buoyancy rise. Finally, understanding and control of plume downwash requires more detailed flow visualization experiments of the vortex structure in the wake behind the bent-over jet from a stack to determine how a plume entrains these down washing vortices, and how stack tips can be designed to discourage the plume from interacting with the vortex field that causes downwash.

3.2. Modeling for cooling tower

Overcamp and Israel [69] had worked on sensitivity analysis of a salt deposition model for natural draft cooling towers. A salt deposition model for natural draft cooling towers was modified so that different modeling assumptions could be tested. These included the method of estimating the effective height of emission of droplets as a function of their size and the use of either a simple trajectory method or a modified Gaussian diffusion-deposition equation for computing the deposition. For this paper, the 22.5° sector-averaged form of the deposition equation developed by Overcamp [70] is applied to estimate the deposition of droplets of a given size:

$$\omega i(x) = \frac{v'_{Di} Q_{Di}(1+\alpha_0)}{(\pi x/8)\sigma_z\sqrt{2\pi u}} \exp\left[-\frac{(h_{Di} - \overline{v'_{Di}}x/u)^2}{2\sigma_z^2}\right] \tag{10}$$

where Q_{Di} is the mass emission of salt in the size interval, v'_{Di}, is the average settling velocity, $\overline{v'_{Di}}$ is the final settling or deposition velocity, and α_0 is partial image coefficient which is defined by:

$$\alpha_0(x) = 1 - \frac{2v'_{Di}}{[v'_{Di} + v'_{Di} + ((u\,h_{Di} - v_{Di}x)/(\sigma_z(x))d\sigma_z/dx]} \tag{11}$$

where h_{Di} is fall the distance. This approach made it possible to determine the effect on the total deposition of changing one component of the model at a time. The comparisons presented show that the use of the trajectory method of computing deposition will result in predictions of total deposition that are nearly the same as those using a Gaussian diffusion 'deposition equation for droplets larger than several hundred micrometers in diameter. The use of the point plume and finite plume formulae which is given by:

$$\Delta h_D = \left(\frac{2}{3\beta^2}\right)^{1/3}\left(\frac{F_o}{uv_D^2}\right) \tag{12}$$

where u is the mean wind speed, β is the entrainment coefficient, and F_o is the initial buoyancy flux which is defined as

$$F_o = g w_o R_o \left[\frac{T_{ov} - T_{av}}{T_{ov}} \right] \quad (13)$$

where T_{ov} and T_{ov} are the virtual temperatures at the exit and in the ambient air, R_o is initial radius and w_o is updraft velocity. Results in similar predictions of the effective height of emission of droplets and of the total salt deposition. On the other hand, the linear plume formula as given by:

$$\Delta h_D = \Delta h \left(\frac{1 - v_D}{w_o} \right) \quad (14)$$

where v_D is settling velocity, Δh_D is the height above the tower when the droplet breaks away from the plume, and Δh is rise of plume gives higher estimates of the effective height of emission for the larger droplets and correspondingly lower predictions of salt deposition close to the tower. The most important result in this study is that the predictions of all models are very sensitive to the emission drift droplet size distribution used for the computation. For natural draft towers, the deposition predictions within the first kilometer or two from the tower are strongly influenced by their size distribution. Because of the difficulty in measuring the emission of the largest droplets, uncertainty as to the accuracy of this size distribution may be a limiting factor in the ability to verify any model with field measurements. It is recommended that only size distributions measured simultaneously with deposition measurements be used in any model verification program. At distances beyond several kilometers from the tower, the predictions using diffusion–deposition equation are relatively insensitive to both the method of estimating the effective height of emission and the drift droplet size distribution. If there is concern about the potential adverse effects of salt deposition only at distances greater than several kilometers from the tower, the drift emission size distribution plays only a minor role in the predictions.

König and Mokhtarzadeh-Dehghan [71] had carried out a numerical study out of three-dimensional, full-scale, turbulent, buoyant plumes from a four-flue chimney in an atmospheric boundary layer. The simulations were based on the k–ε turbulence model and a finite volume method. The investigation was aimed to verify the question of how closely the overall characteristics of merged plumes from a multi-flue chimney match those of an equivalent single plume. Therefore, the results for multi flue plumes were compared with those for a single plume under the same release conditions for volume flow rate, momentum and temperature. The differences in the velocity, temperature and turbulence energy fields of a single plume and multiple plumes were mainly significant in the early stages of rise and spreading. Due to the differences in the values for k between the three cases in this region, concentration fluctuations of released chemicals in reacting plumes may get wrongly predicted (depending on the prevailing wind direction) when a multi flue chimney is modeled as a single flue chimney. The larger drop in 'k' and the smaller plume width, the single plume experiences greater lateral changes than the multiple plumes, as can be seen in Figs. 16–18. By ten diameters downstream of the chimney, the multiple plumes are already merged into a single plume and the plume's cross-sections for all three cases become very similar. The multi flue plumes undergo greater changes in the early stages of rise and spreading compared with single plumes. If the flue duct arrangement within the chimney relative to the cross-wind is such that one plume shields another plume (as in case A), then the latter plume is able to initially rise higher and this leads to an overall increase in the rise height of the merged plumes. If the arrangement of the flues is such that the cross-wind is able to penetrate between the plumes (as in case B), then the resulting merged plumes will have a reduced rise height. The single flue case C and the multi flue case A provide the same degree of overall resistance to the cross flow and thus show closer similarities than with case B. Therefore, there is a close agreement between the rise height of the single flue plume and multiple flue plume of case A. The merged plumes of case B remain lower (approximately 1D) throughout the spreading.

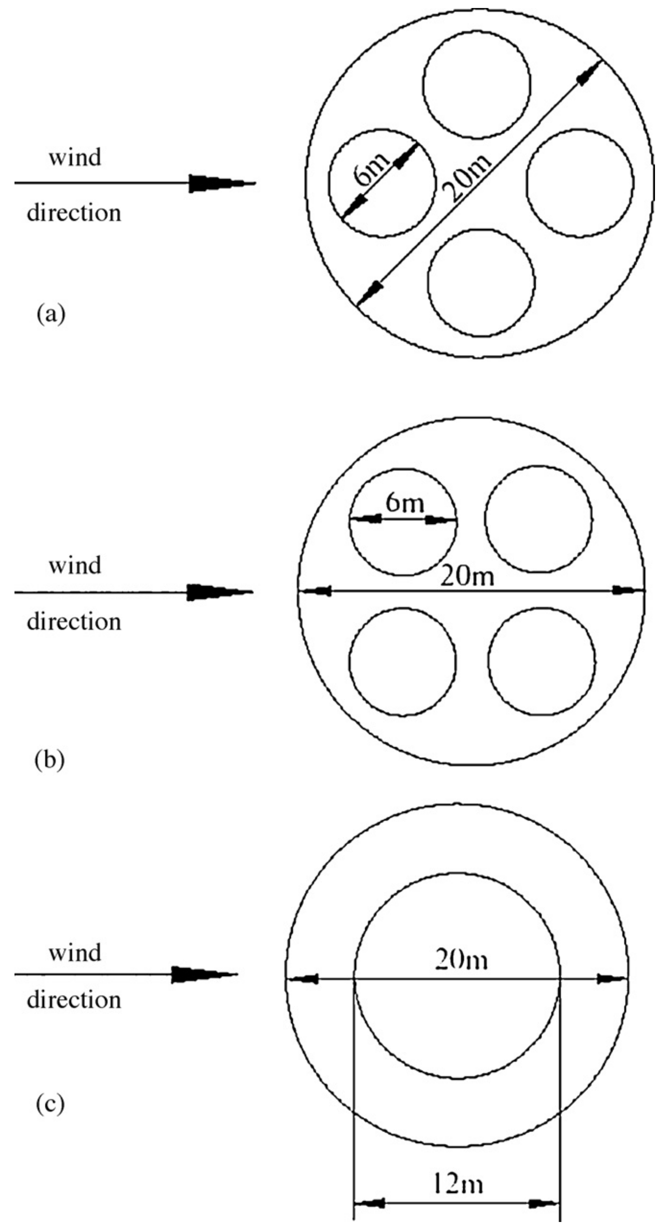


Fig. 16. Cases studied: (a) multi flue case A; (b) multi flue case B; and (c) single flue case C.

Mokhtarzadeh-Dehghan et al. [72] numerical study of single and two interacting turbulent plume in atmospheric cross flow. The study simulates plumes from a mechanical draught cooling tower. The plumes are placed in tandem or side-by-side. The cooling tower geometries are shown in Fig. 19. The diameter of the plume source and the height of the tower are based on the dimensions of a real mechanical draught cooling tower. Results are first presented for plumes with a density ratio of 0.74 and plume-to-crosswind speed ratio of 2.33, for which data from a small-scale wind tunnel experiment were available and were used to assess the accuracy of the numerical results. Further results are then presented for the more physically realistic density ratio of 0.95, maintaining the same

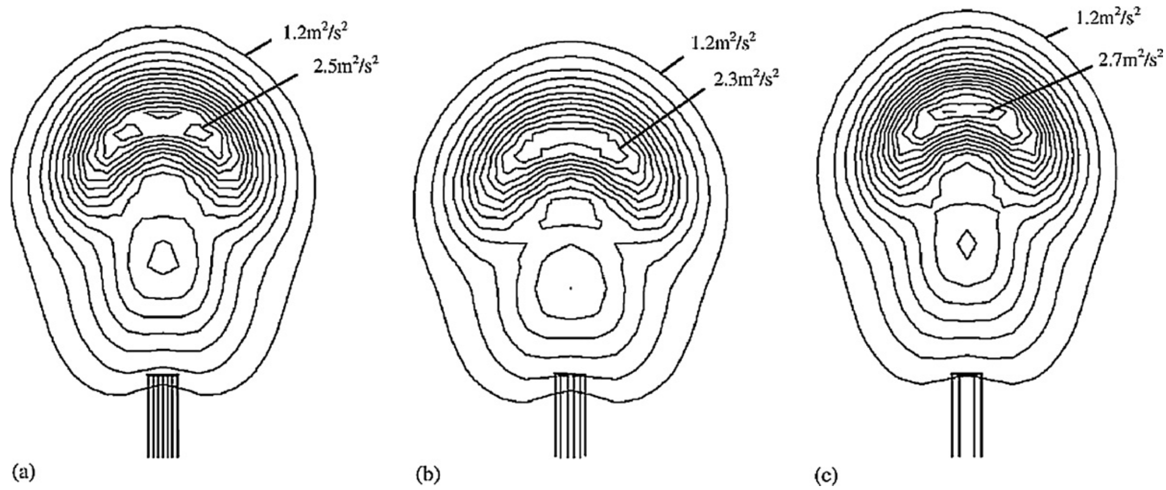


Fig. 17. Turbulence energy fields at $x = 2D$: (a) case A; (b) case B; (c) case C. Contour interval 0.5 $m^2\ s^{-2}$.

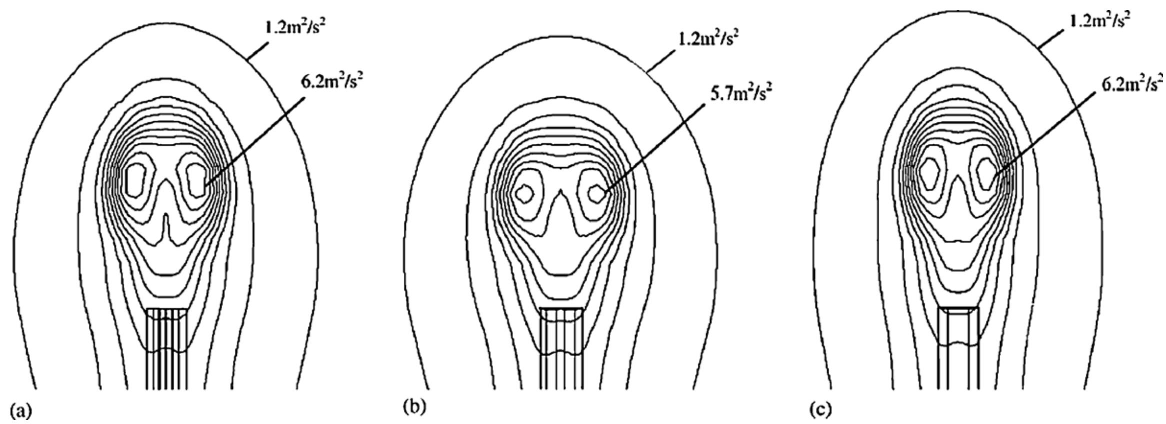


Fig. 18. Turbulence energy fields at $x = 10D$: (a) case A; (b) case B; (c) case C. Contour interval 0.1 $m^2\ s^{-2}$.

Table 4
Constants in turbulence models.

	Standard k–ε	RNG k–ε	Differential flux model	Reference
C_μ	0.09	0.085	–	Eddy viscosity formula
C_1	1.44	1.42	1.44	ε-Equation
C_2	1.92	1.68	1.92	ε-Equation
C_3	1.0	1.0	1.0	Buoyancy term
β		0.015	–	RNG model
η_0		4.38		RNG model
C_{1S}, C_{2S}, C_{3S}	–	–	1.8, 0.6, 0.5	Reynolds stress equations
C_{1F}, C_{2F}, C_{3F}	–	–	3.0,0.5,0.33	Reynolds flux equations
Turbulent Prandtl number	$\sigma_k = 1.0$	$\sigma_k = 0.7179$		k-Equation
	$\sigma_\varepsilon = 1.217$	$\sigma_\varepsilon = 0.7179$		ε-Equation
			$\sigma_{DS} = 1.0$	Reynolds stress
	0.9	0.9	$\sigma_{DF} = 1.647$	Reynolds heat fluxes
			0.9	Enthalpy

speed ratio. It was shown that a tandem arrangement led to significant increase in rise height and the merging of the plumes occurred by 40D downstream of the source. For a distance of 1D between the side-by-side plumes in the present study, merging of the plumes was slow and complete merging did not take place by 40D. It was concluded that the penetration of the crosswind between the two plumes played a major role in this case. The sensitivity of the results with respect to three turbulence models, namely, the standard k–ε

Table 5
Turbulence models and discretisation schemes.

u, v, w	P	k, ε	h	Reynolds stresses	heat fluxes	Cases
k–ε	HD	CD	HD	HD	–	S, T, SBS
k–ε RNG	HD	CD	HD	HD	–	S, T, SBS
DFM	UD	CD	HD	HD	HD	S, T, SBS
k–ε	QUICK	CD	QUICK		–	S, T, SBS

HD, hybrid; CD, central difference; UD, upwind; S, single plume; T, plumes in tandem; SBS, side-by-side plumes.

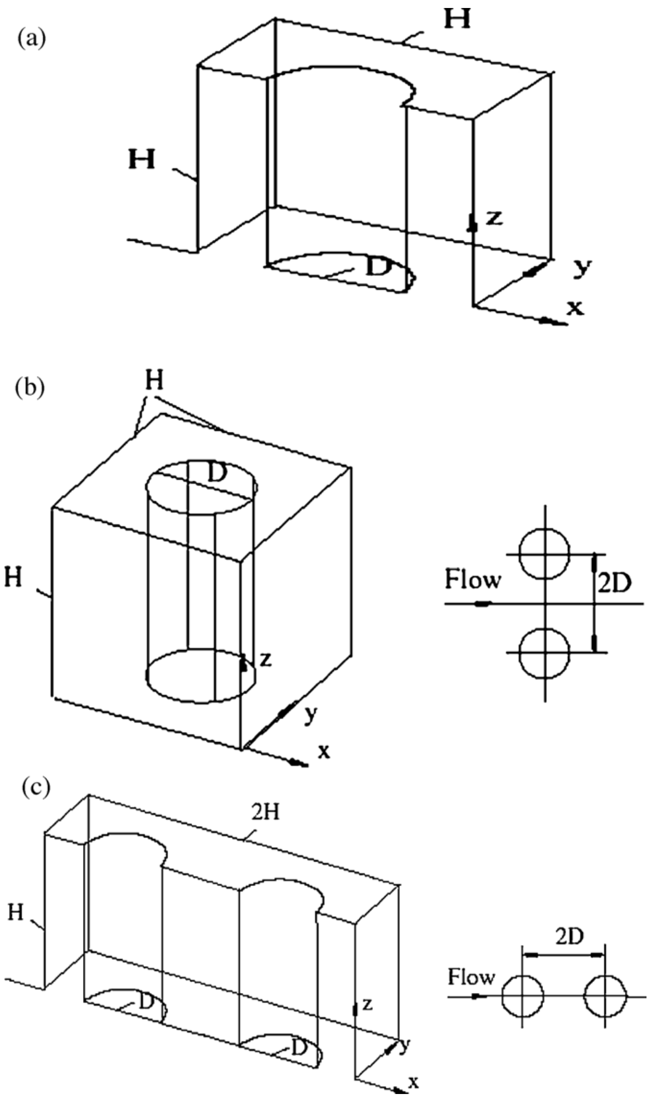


Fig. 19. Cooling tower geometries (D = 10 m, H = 20 m): (a) single source; (b) side-by-side sources de sources; and (c) tandem sources.

model, the RNG k–ε model and the differential flux model (DFM) had been presented (Tables 4 and 5). Comparisons are also made between the predicted rise height and the values obtained from existing integral models. The formation of two counter-rotating vortices is well predicted. The results show good agreement for the rise height predicted by different turbulence models, but the DFM predicts temperature profiles more accurately. For tandem plumes, the enhancement factor was greater than the theoretical value for maximum enhancement. For the side-by-side plumes, there was a negative enhancement at large distance of 40D, in agreement with the experimental data. The tandem arrangement, therefore, resulted in greater differences.

Meroney [73] worked on protocol for computational fluid dynamics prediction of cooling-tower drift in an urban environment. In this study a computational fluid dynamics (CFD) code including Lagrangian prediction of the gravity driven but stochastic trajectory descent of droplets has been considered to predict plume rise and surface drift deposition from mechanical draft cooling towers. The CFD drift deposition calculations were performed for a specific urban cooling-tower situation with and without the urban buildings surrounding the cooling-tower complex to produce a set of multiplicative factors that could be used to correct seasonal or annual predictions for the presence of large urban structures. They

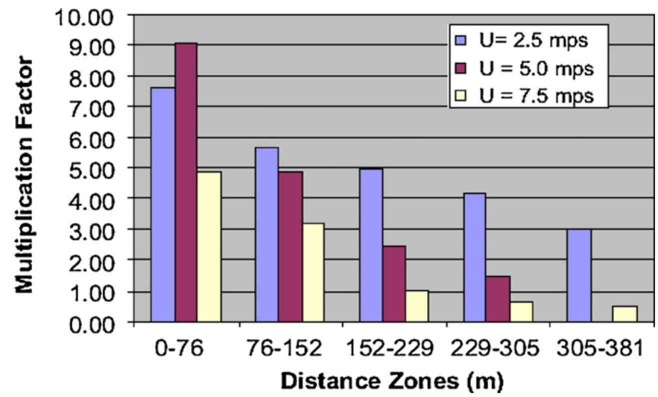


Fig. 20. Zonal MF 160°, U = 2.5–7.5 mps.

performed zonal calculations for four wind orientations (160°, 180°, 220°, and 240°), three wind speeds (2.5, 5.0, and 7.5 m/s measured at a height of 52 m with a velocity profile power law coefficient equal to 0.25), and droplets were emitted vertically in a air/vapor plume at 8.5 m/s from the cooling-tower units 1 through 11 at a rate of 1 kg/s and a Rosin–Rammler droplet distribution (characterized by a mean diameter of 0.1 mm, a minimum diameter of 0.01 mm, a maximum diameter of 1 mm, and a shape factor, n, equal to 1.0). Mass deposition rates (kg/s) were calculated for each zone for the four wind orientations, 160°, 180°, 220°, and 240°, respectively. Typical results for a reference wind speed, U = 5 m/s were shown in Table 6 for isolated cooling tower and cooling tower surrounded by a full set of buildings for four wind orientations. The difference between the values recorded for total trapped and trapped ground reflects deposition directly on the sides and roofs of buildings. Given the random number methodology used in the stochastic discrete particle method to generate particle paths, it was found that individual replications of deposition may vary ±30% around the average, but deposition trends are consistent.

3.2.1. Multiplication factors

The ratio of the mass accumulation rate for a given zone and a fully configured building case to the mass accumulation for the equivalent zone and the isolated cooling-tower facility case is designated here as a deposition multiplication factor (MF). Table 7 displays the MF values for the four wind orientations, 160°, 180°, 220°, and 240°, respectively. Figs. 20–23 display similar information in the form of bar charts. MF appears to be largest for the 160° and 240° orientations.

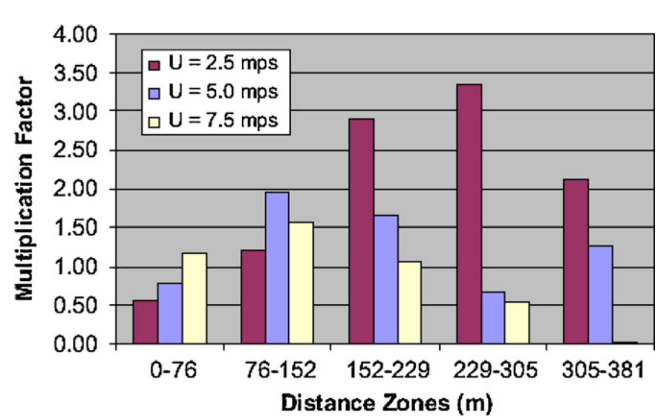


Fig. 21. Zonal MF 240°, U = 2.5–7.5 mps.

Table 6
Zonal deposition rates, $U = 5$ m/s, distances measured downwind of CT and boiler downwind edge.

Arrangement	Isolated CT	Isolated CT	Isolated CT	Isolated CT	Structures Present	Structures Present	Structures Present	Structures Present
Wide angel	160°	180°	220°	240°	160°	180°	220°	240°
Distance, m (ft)	Mass rate (kg/s)	Mass rate (kg/s)	Mass rate (kg/s)	Mass rate (kg/s)	Mass rate (kg/s)	Mass rate (kg/s)	Mass rate (kg/s)	Mass rate (kg/s)
−305 to 0 (−1000 to 0)	0.0000	0.0102	0.0591	0.0000	0.0960	0.0740	0.1150	0.0780
0–76 (0–250)	0.0138	0.0491	0.0987	0.0815	0.1250	0.0955	0.0780	0.1290
76–152 (250–500)	0.0224	0.0381	0.0382	0.0371	0.1090	0.0666	0.0750	0.1180
152–299 (500–750)	0.0283	0.0306	0.0260	0.0143	0.0685	0.0336	0.0430	0.0400
229–305 (750–1000)	0.0152	0.0294	0.0136	0.0187	0.0220	0.0357	0.0090	0.0330
305–381 (1000–1250)	–	0.0155	0.0119	0.0197	0.0220	0.0194	0.0150	0.0100
CT and boiler roofs	0.0171	0.0632	0.0873	0.1260	0.1260	0.1850	0.1460	0.1130
Downwind outlet	0.9030	0.7639	0.6652	0.7100	0.4260	0.4820	0.5160	0.4710
Total trapped	0.0968	0.2361	0.3348	0.2973	0.5685	0.5098	0.4810	0.5210
Trapped ground	0.0797	0.1627	0.2884	0.1713	0.3465	0.2508	0.2200	0.3300
Mass balance	0.9998	1.0000	1.0000	1.0073	0.9945	0.9918	0.9970	0.9920

Table 7
Multiplication factors (MF), $U = 5$ m/s.

Distance, m (ft)	MF 160°	MF 180°	MF 220°	MF 240°
0–76 (0–250)	9.06	1.951	0.79	1.58
76–152 (250–500)	4.87	1.75	1.96	3.18
152–229 (500–750)	2.42	1.10	1.65	2.80
229–305 (750–1000)	1.45	1.21	0.66	1.76
305–381 (1000–1250)	–	1.25	1.26	0.51
Average	4.45	1.45	1.27	1.97
Total trapped	5.87	2.16	1.44	1.75
Trapped ground	4.35	1.54	1.17	1.93

Table 8
Average multiplication factors (AMF).

Velocities	AMF 160°	AMF 180°	AMF 220°	AMF 240°
$U = 2.5$ mps	5.60	–	–	2.03
$U = 5.0$ mps	4.45	1.45	1.27	1.97
$U = 7.5$ mps	4.40	–	–	1.09
Average	4.82	1.45	1.27	1.69

3.2.2. *Average MF*

If one averages the five zonal deposition MF one obtains the average multiplication factor (AMF) for a given wind orientation. Table 8 displays the predicted influence of approach wind speed on zonal deposition through the AMF. A protocol is proposed to generate a typical set of coefficients that might be used to adjust the results of seasonal or annual deposition predictions using analytic programs such as ISC Prime or SATCI. The multiplicative and average multiplicative factors (MF and AMF) produced are based on reasonable scientific certainty concerning the physics of the fluid processes and the analytic and computational methods employed.

3.3. *Modeling for chiller*

3.3.1. *System description and analysis*

There is a central air conditioning system, containing six water cooled chillers and ten wet cooling towers, besides other

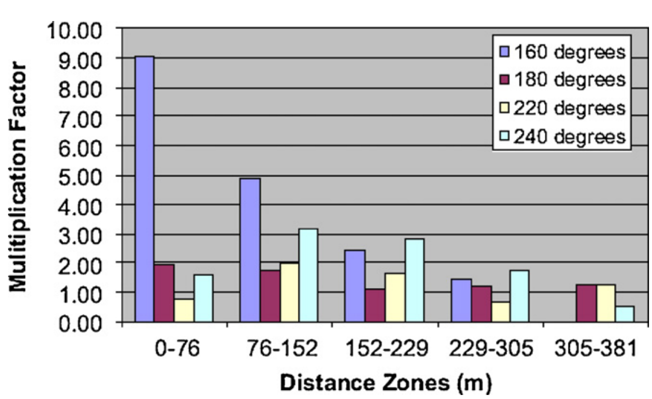


Fig. 22. Zonal MF 160–240°, $U = 5$ mps.

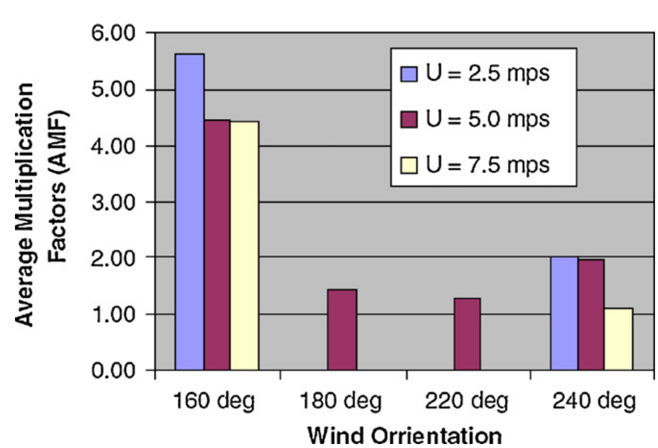


Fig. 23. Zonal AMF, 160–240°, $U = 2.5$–7.5 mps.

equipments such as, the heat exchangers, connecting pipes, and pumps. Since the schematic diagram of the entire system is too complex to design in a compact figure, so a simple line diagram is given in Fig. 7(a). The complete line diagram ((Fig. 7(a)) consists of a chiller coupled with a building envelope (space to be cooled), a cooling tower (to extract heat from the chiller) and a heat pump/solar collector (to heat the exhaust of the cooling tower). As can seen from Fig. 7(a), the refrigerant absorbs the heat from the evaporator and changes from saturated liquid state to saturated vapor state and enter the compressor, where it is compressed up to (superheated) state point 2. At state point 2 the refrigerant enters the condenser and cools down up to state point 3 (saturated liquid) by rejecting the heat to the circulating water from the cooling tower. At state point 3, it enters the expansion valve and being expanded up to state point 4 and again enters the evaporator, thereby, completing the chiller sub-system.

The water entering the condenser at state point 8 absorbs the heat from the refrigerant rejected in the condenser and then pumped back to the cooling tower at state point 6. The hot water at state point 6 is sprayed over the fill packing, and comes in the contact of the ambient air being circulated by the exhaust fan on the top of the cooling tower shown in Fig. 7(a). The hot water cooled down up to state point 8 and the heat is taken away by the ambient air through evaporative cooling. The air entering the cooling tower through side openings leaves the tower through the exhaust fan via a duct at state point 7, completing the cooling tower sub-system. On the other hand, the circulating water leaving the evaporator at state point 10 enters the cooling coil where the secondary fluid is circulated to cool down the building space and the higher temperature water is pumped back to the evaporator at state point 9, thereby, completing the building sub-system. The analysis of main sub-systems viz. the chiller and cooling tower along with the heating and cooling requirements (in brief) is given as below:

3.3.2. Chiller simulation

The chiller model simulates the chiller performance under various working conditions on the base of impeller tip speed (u_2), impeller exhaust area (A), impeller blades angle (β) and thirteen other coefficients/constants. This might be available from chiller technical data and/or can be identified (partially or fully) by an associated pre-processor using chiller performance data under full load and partial load. The chiller chilling capacity is assumed to be controlled by adjusting the inlet vane angle (θ), the refrigeration cycle of a two-stage centrifugal chiller model was given by Wang et al. [74]. The compressor is modeled on the basis of mass conservation, Euler turbo-machine and energy balance equation. The Euler equation is modified by considering the impeller exit radial velocity (c_{r2}) distribution and derived as:

$$h_{th} = u_2 \left[u_2 - \left(\frac{\pi^2}{8} \right)^2 c_{r2} \left(ctg\beta + B \frac{v_1}{v_i} tg\theta \right) \right] \tag{15}$$

where h_{th} is theoretical head, B is the ratio of impeller channel depth at intake to that at exhaust, v_1 and v_i are specific volume at impeller intake and exhaust respectively. Energy balance equations are applied on two control volumes, i.e. compressor control volume (from compressor suction to compressor exhaust) and impeller control volume (from compressor suction to impeller exit) as given by Eqs. (16) and (17).

$$h_{th} = h_{pol.comp} + h_{hyd.comp} \tag{16}$$

$$h_{th} = h_{pol.imp} + h_{hyd.imp} + \frac{c_i^2}{2} \tag{17}$$

where h_{pol} is polytrophic compression work, h_{hyd} is hydrodynamic losses, c_i is the vapor velocity at impeller exhaust. The hydrodynamic losses in two control volumes are considered to be composed of three elements (i.e. flow friction losses, inlet losses and incidence losses) as given by Eqs. (18) and (19).

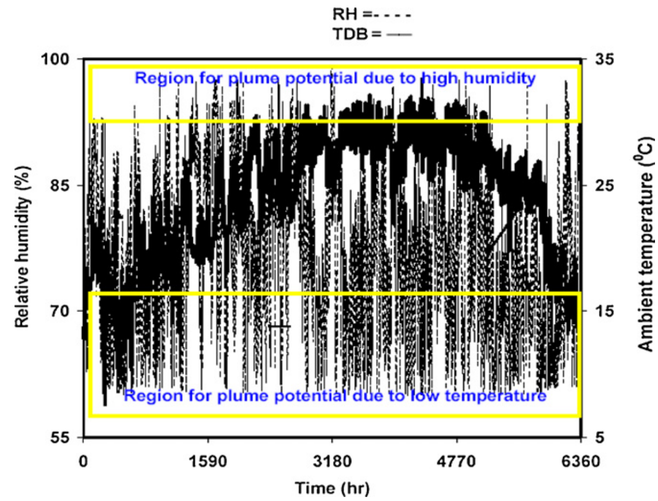


Fig. 24. Hourly variation of relative humidity and ambient air temperature for a typical year in Hong Kong.

$$h_{hyd.comp} = \varsigma \left[1 + \psi_1 \left(\frac{v_1}{v_i} \frac{1}{\cos\theta} \right)^2 + \psi_2 \left(\frac{v_1}{v_i} tg\theta \right)^2 \right] c_{r2}^2 \tag{18}$$

$$h_{hyd.imp} = \varsigma \left[\chi + \psi_1 \left(\frac{v_1}{v_i} \frac{1}{\cos\theta} \right)^2 + \psi_2 \left(\frac{v_1}{v_i} tg\theta \right)^2 \right] c_{r2}^2 \tag{19}$$

where ζ, ψ_1, ψ_2, χ are the introduced constants. The flow friction losses are considered to be proportional to the square of the compressor volume flow rate and hence, proportional to the square of the impeller exit radial velocity (c_{r2}^2). The inlet losses are considered to be proportional to the square of the velocity through pre-rotation vanes channel. The incidence losses are considered to be proportional to the square of the shock velocity component. Given the evaporator pressure, condenser pressure and position of inlet vanes (value of θ), the compressor model can calculate radial velocity and specific volume at impeller exhaust, and hence, the refrigerant mass flow rate and internal power consumption. The compressor capacity is controlled by the inlet vanes angle (θ) as given in Eqs. (18) and (19).

For multi-stage chillers, single stage compressor equations are used to calculate the first stage. The second stage is assumed to have the same flow, efficiency and compression ratio as the first stage. Mass and energy conservations are applied to the economizer and the mixing process at the second stage suction. Only the first stage impeller geometric parameters are of concern. The evaporator and the condenser are simulated using the classical heat exchanger efficiency method. By considering the effects of water flow rate ($M_{w,ev}$, $M_{w,cd}$) and heat flux (Q_{ev}, Q_{cd}), the evaporator and condenser overall heat transfer coefficient-area products (UA_{ev}, UA_{cd}) are represented empirically, by Eqs. (20) and (21).

$$UA_{ev} = [C_1 M_{w,ev}^{-0.8} + C_2 Q_{ev}^{-0.745} + C_3]^{-1} \tag{20}$$

$$UA_{cd} = [C_4 M_{w,cd}^{-0.8} + C_5 Q_{cd}^{1/3} + C_6]^{-1} \tag{21}$$

where C_1–C_6 are constants, the evaporation and condensation temperatures, and hence, the evaporator and condenser pressures are calculated, for the given chiller capacity (Q_{ev}), heat rejection (Q_{cd}), chilled and cooling water flow rates and inlet temperatures.

The power consumption of the chiller (W) is calculated on the basis of the compressor internal power consumption (W_{in}). With

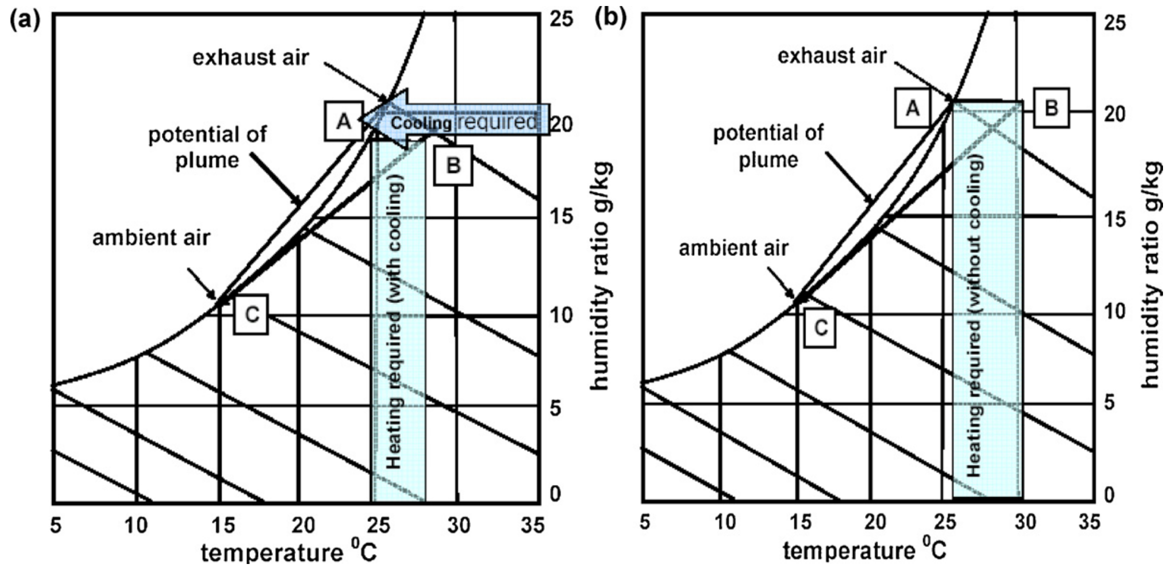


Fig. 25. The heating and cooling requirements for a typical cooling tower (a) with cooling option and (b) without cooling option.

the consideration of mechanical and leakage losses of the compressor, electrical and mechanical losses of the motor, the chiller power consumption, can be calculated by Eq. (22).

$$W = \alpha \times W_{in} + W_l \quad (22)$$

where α is a coefficient.

3.3.3. Cooling tower simulation

The cooling tower model is used to simulate the states of outlet air and outlet water of the cooling tower. In this simulation, the effectiveness model for cooling towers developed by Braun [6] is used. Based on the steady-state energy and mass balance on an incremental volume, the following differential equations can be derived.

$$dm_w = m_a d\omega_a \quad (23)$$

$$\frac{dT_w}{dV} = \frac{(dh_a/dV) - C_{pw}(T_w - T_{ref})(d\omega_a/dV)}{[(m_{w,i}/m_{a)} - (\omega_{a,o} - \omega_a)]C_{pw}} \quad (24)$$

where m_w is mass flow rate of water, m_a is mass flow rate of dry air, ω_a is air humidity ratio, h_a is enthalpy of moist air per mass of dry air, C_{pw} is specific heat of water at constant pressure, T_{ref} is reference temperature for zero enthalpy of liquid water. The effectiveness of cooling tower is used to simulate the heat and mass transfer processes in the cooling tower as given in Eq. (25).

$$Q = \varepsilon_a m_a(h_{s,w,i} - h_{a,i}) \quad (25)$$

where ε_a is air side heat transfer effectiveness, $h_{a,i}$ is the enthalpy of inlet moist air per mass of dry air, $h_{s,w,i}$ is the saturation air enthalpy with respect to the inlet temperature of water surface. The outlet air state and water state can be determined through energy balance as given by Eqs. (26)–(28).

$$h_{a,o} = h_{a,i} + \varepsilon_a(h_{s,w,i} - h_{a,i}) \quad (26)$$

$$\omega_{a,o} = \omega_{s,w,e} + (\omega_{a,i} - \omega_{s,w,o})\exp(-NTU) \quad (27)$$

$$T_{w,o} = T_{ref} + \frac{m_{w,i}(T_{w,i} - T_{ref})C_{pw} - m_a(h_{a,o} - h_{a,i})}{m_{w,o}C_{pw}} \quad (28)$$

3.3.4. Requirements of heating and cooling

For a typical weather conditions, the formation and the potential of visible plume are shown in Fig. 7(b) and (c), while the hourly ambient air temperature and relative humidity is shown in Fig. 24. Since, the present method based is a technique to cool and then heat and/or to heat the exhaust of the cooling tower, so the requirements of heating and cooling as well as heating are shown in Fig. 25(a)–(b) respectively. This is clear from these figures that the heating is carried out in a way the exhaust of the tower while mixing with the ambient air along the line B to C remains in the sub saturated region as also mentioned in Fig. 7(b). The straight line AB (Fig. 25(a) and (b)) shows the requirements of heating, while the line AC through the saturation curve shows the cooling pattern. The heating and cooling requirements are given by the following equations.

$$Q_H = \dot{m}_a C_{pa}(T_{aa} - T_{set}) \quad (29)$$

$$Q_L = \dot{m}_a C_{pa}(T_{set} - T_{aset}) \quad (30)$$

where $\dot{m}_a$ and C_{pa} are respectively the mass rate and specific heat of the tower exhaust air, while T_{aa}, T_{set} and T_{aset} are, respectively, the outlet, set point and the adjusting set point temperatures of the exhaust air to be heated and/or to be cooled down in order to control the visible plume. All other parameters can be measured directly from the system and/or calculated by the models given above. But T_{set} and T_{aset} need to be calculated based on the exhaust and inlet air temperatures of the cooling tower by plotting (on the psychrometric chart) as mentioned in the text and shown in Fig. 25(a) and (b), respectively. Again, based on the total heating requirement, the cooling can be calculated by the ratio of the heating to the cooling (Q_H/Q_L) of the heat pump installed for this purpose. On the other hand, the requirement of the heating can be calculated directly from Fig. 25(b).

4. Conclusions

The following conclusions can be drawn from the study of formation potential and analysis of cooling tower plumes:

- Recently study on application of plume control from wet cooling towers of commercial buildings has been done which shows that, solar collector can be an alternative but may not be a substitute provided weather condition is not a big constraint.
- Study on evaluation of alternative arrangements of a heat pump for plume abatement in a large scale chiller plant in a subtropical region had been done which shows that, utilization of chilled water as the heat source of the heat pump system for plume

control is more preferable for improving the overall energy efficiency than utilization of cooling water as the heat source.

- Various mathematical models has been developed for the numerical analysis of cooling tower plumes, closed form integration model (CFIM) simulates the observed visible plume behavior reasonably well.
- For solar collector system, the fuel (the sun light) is free and the investment cost is very less as compared to those of the heat pump systems and hence, the former is much cheaper than the later. Again, the running cost for the solar collector systems is nominal as compared to those of different heat pump systems and can be a better option from the point of view of economics as well as from the point of view of thermodynamics. So the application of solar collectors can be an alternative but may not be a substitute provided, weather condition is not a big constraint.
- The combined heating and cooling option is feasible only in the case of heat pump systems and hence, the solar collector cannot be used for dual application. The combined option not only consumes less energy but also utilizes the cooling produced by the heat pump system and hence, the combined option is more economical that the heating alone option especially in the case of heat pump systems. Also the temperature of the refrigerant is much higher at the exit of the compressor, i.e. at the entering of the condenser. So a desuperheater can be used to utilize the heat produced by the condenser, especially, where there is no need of heating the building such as Hong Kong.

Acknowledgements

One of the authors (AKP) gratefully acknowledges the financial assistance in the form of National Renewable Energy Fellowship due to Ministry of New & Renewable Energy, Government of India, New Delhi, India.

References

[1] Lewis WK. The evaporation of liquid into gas. Trans ASME 1922;44:325–40.
[2] Robinson CS. The design of cooling towers. Mech Eng 1923;15:99–102.
[3] Merkel F. Verdunstungskiihung, VDI Forschungsar beiten, No. 275. Berlin, Germany; 1925.
[4] Baker DR, Shrylock HA. A comprehensive approach to the analysis of cooling tower performance. J Heat Transfer 1961;83:339–49.
[5] Sutherland JW. Analysis of mechanical draught counter flow air water cooling towers. ASME Trans 1983;105:576–83.
[6] Braun JR. Methodologies for the design and control of central cooling plant. Ph.D. thesis. University of Wiscosin, Madison; 1988.
[7] Braun JR, Klein S, Mitchell J. Effectiveness model for cooling towers and cooling coils. ASHRAE Trans 1989;95:164–74.
[8] Shelton SV, Weber ED. Modeling and optimization of a commercial building chillers/cooling tower systems. ASHRAE Trans 1991;97:1209–16.
[9] Lebrun J. A toolkit for primary HVAC energy calculations. Atlanta: ASHRAE Inc.; 1993.
[10] Bernier MA. Cooling tower performance – theory and experiments. ASHRAE Trans 1994;100:114–21.
[11] Lebrun J, Silva CA. Cooling towers – model and experimental validation. ASHRAE Trans 2002;108:751–9.
[12] Naphon P. Study on the heat transfer characteristics of an evaporative cooling tower. Int Commun Heat Mass Transfer 2005;32:1066–74.
[13] Kloppers JG, Kröger DG. A critical analysis into the heat and mass transfer analysis of counter flow wet-cooling tower. Int J Heat Mass Transfer 1998;48:765–77.
[14] Kloppers JG, Kröger DG. Cooling tower performance evaluation: Merkel, Poppe and e-NTU methods of analysis. J Eng Gas Turbine Power 2005;127:1–7.
[15] Kloppers JG, Kröger DG. The Lewis factor and its influence of the performance prediction of wet-cooling towers. Int J Therm Sci 2005;44:879–84.
[16] Lees M. The economics of wet versus dry cooling for combined cycle. In: IMechE, Symposium on condenser and cooling towers for combined cycle. 1994.
[17] Smith WW. Prediction of cooling tower performance. ASHRAE Trans 1954;6:27–36.
[18] ASHRAE. ASHRAE handbook-HVAC systems and equipments. ASHRAE Inc.; 1996 [chapter 36].
[19] Bouton F, Winter RJ. Mechanical drought cooling towers with visible plume abatement. In: Inst IMechE, Second Seminar on CCGT. 1992.
[20] Bennett M, Sutton S, Gardiner DRC. An analysis of lider measurements of buoyant plume rise and dispersion at five power stations. Atmos Environ 1992;26A:3249–63.
[21] Fisher BEA. Predicting cooling tower plume dispersion. In: Symposium on condenser and cooling towers for combined cycle, Int. IMechE. 1994.
[22] Winter RJ. Control of visible plumes form cooling towers. Proc Inst Mech Eng 1997;211A:67–72.
[23] Fisher BEA. Predicting cooling tower plume dispersion. Proc Inst Mech Eng 1997;211A:291–7.
[24] Corti A, Carnevale E. Environmental impact from wet plume in combined cycle power plants. Appl Therm Eng 1998;18:1049–57.
[25] Foster PM. Droplet growth inside and outside cooling towers. II. Calculation of droplet fallout from cooling tower plumes. Atmos Environ 1974;8:393–402.
[26] Slawson PR. Observation and prediction of natural draft cooling tower plumes at paradise steam plant. Atmos Environ 1977;12:1713–24.
[27] Dittenhoefer CA, Pena D, Rosa G. A study of production and growth of sulfate particles in plumes from a coal-fired power plant. Atmos Environ 1978;12:297–306.
[28] Köenig RL. Anomalous snowfall caused by natural-draft cooling towers. Atmos Environ 1981;15(7):1117–28.
[29] Spillane KT, Elsum CC. Prediction of cloud effects in chimney plumes. Atmos Environ 1982;17(5):983–90.
[30] Splilane KT, Elsum CC. Convective knock-down of cooling tower plumes. Atmos Environ 1983;17(2):227–33.
[31] Overcamp TJ, Hoult DP. Precipitation in the wake of cooling towers. Atmos Environ 1971;5:751–66.
[32] Barber FR, Martin A, Shepherd JG, Spurr G. The persistence of plumes from natural draft cooling towers. Atmos Environ 1974;8:407–18.
[33] Moore DJ. Recent Central Electricity Generating Board research on environmental effects of wet cooling towers, Cooling Tower Environment-1974. U.S. Energy Research and Development Administration; 1975. p. 205–19.
[34] Campistron B. Interaction between a natural snowfall and a cooling tower plume: an experimental study with a millimetric Doppler radar. Atmos Environ 1987;21(6):1375–83.
[35] Huff FA. Potential augmentation of precipitation from cooling tower effluents. Bull Am Met Sot 1972;53:639–44.
[36] Schatzmann M, Lohmeyer A, Ortner G. Flue gas discharge from cooling towers – wind tunnel investigation of building downwash effects on ground level concentrations. Atmos Environ 1987;21(8):1713–24.
[37] Majumdar S, Rodi W. Three-dimensional computation of flow past cylindrical structures and model cooling towers. Build Environ 1989;24(1):3–22.
[38] Wei QD, Zhang B, Liu K, Du X, Meng DXZ. A study of the unfavorable effects of wind on the cooling efficiency of dry cooling towers. J Wind Eng Ind Aerodyn 1995;54/55:633–43.
[39] Derksen DD, Bender TJ, Bergstrom DJ, Rezkallah KS. A study on the effects of wind on the air intake flow rate of a cooling tower. Part I. Wind tunnel study. J Wind Eng Ind Aerodyn 1996;64:47–59.
[40] Macdonald RW, Strom RK, Slawson PR. Water flume study of the enhancement of buoyant rise in pairs of merging plumes. Atmos Environ 2002;36: 4603–15.
[41] Briggs GA. Plume rise predictions. In: Lectures on air pollution and environmental impact analyses. Boston, MA: American Meteorological Society; 1975. p. 59–111.
[42] Briggs GA. Plume rise from multiple sources. In: Cooling Tower Environment-1974, ERDA Symposium Series, CONF-740302. National Technical Information Service; 1975. p. 161–79.
[43] Murphy BL. Plume rise from a row of chimneys. Presented at the 68th annual meeting of the air pollution control association, Paper No. 75-04.7. Boston, MA, 15–29 June; 1975.
[44] Anfossi D, Bonino G, Bossa F, Richiardone R. Plume rise from multiple sources: a new model. Atmos Environ 1978;12:1821–6.
[45] Tyagi SK, Wang SW, Ma ZJ. Prediction, potential and control of plume from wet cooling tower of commercial buildings in Hong Kong: a case study. Int J Energy Res 2007;31:778–95.
[46] Wang SW, Tyagi SK, Sharma A, Kaushik SC. Application of solar collectors to control the visible plume from wet cooling towers of a commercial building in Hong Kong: a case study. Appl Therm Eng 2007;27:1394–404.
[47] Gao M, Sun FZ, Wang K, Shi Y-t, Zhao Y-b. Experimental research of heat transfer performance on natural draft counter flow wet cooling tower under cross-wind conditions. Int J Therm Sci 2008;47:935–41.
[48] Tyagi SK, Wang SW, Park SR, Sharma A. Economic considerations and cost comparisons between the heat pumps and solar collectors for the application of plume control from wet cooling towers of commercial buildings. Renew Sust Energy Rev 2008;12:2194–210.
[49] Xu X, Wang S, Zhenjun M. Evaluation of plume potential and plume abatement of evaporative cooling towers in a subtropical region. Appl Therm Eng 2008;28:1471–84.
[50] Sarker MMA, Kim E, Moon CG, Yoon JI. Performance characteristics of the hybrid closed circuit cooling tower. Energy Build 2008;40:1529–35.
[51] Wang J, Wang S, Xu X, Xiao F. Evaluation of alternative arrangements of a heat pump system for plume abatement in a large-scale chiller plant in a subtropical region. Energy Build 2009;41:596–606.
[52] Lucas M, Martínez PJ, Ruiz J, Kaiser A, Viedma A. On the influence of psychrometric ambient conditions on cooling tower drift deposition. Int J Heat Mass Transfer 2010;53:594–604.
[53] Policastro AJ, Dunn WE, Berg ML, Ziebarth JP. The chalk point dye tracer study: validation of models and analysis of field data. In: Lee SS, Sengupta S, editors. Proceedings of second conference on waste heat management and utilization. 1978. p. 686–719.

[54] Policastro AJ, Dunn WE, Breig M, Ziebarth J. Comparison of ten drift deposition models to field data acquired in the chalk point dry tracer experiment. In: Environmental effects of cooling tower plumes, symposium on (supplement) University of Maryland. 1978. p. 76–84.
[55] Meroney RN. CFD prediction of cooling tower drift. J Wind Eng Ind Aerodyn 2006;94:463–90.
[56] Al-Waked R. Crosswinds effect on the performance of natural draft wet cooling towers. Int J Therm Sci 2010;49:218–24.
[57] Chen Norbert CJ, Jung L. A mathematical model of drift deposition from a bifurcated cooling tower plumes. Atmos Environ 1977;12:1969–80.
[58] Golay MW. Numerical modeling of buoyant plumes in turbulent, stratified atmosphere. Atmos Environ 1983;16(10):2371–81.
[59] Csanady G. Turbulent diffusion in the environment. Holland: D. Reidel; 1973.
[60] Overcamp TJ, Kut T. Effects of a virtual origin correction on entrainment coefficients as determined from observations of plume rise. Atmos Environ 1986;20(2):293–3133.
[61] Slawson PR, Rennie JH. Some observations on moist plume behavior at a pilot stack facility. Waterloo, Ontario: Department of Mechanical Engineering, University of Waterloo; 1971.
[62] Wright SJ. Mean behavior of buoyant jets in a crossflow. J Hydr Div ASCE 1977;103:499–513.
[63] Wright SJ. Effects of ambient cross flows and density stratification on the characteristic behavior of round turbulent buoyant jets. Report KH-R-36. Pasadena, CA: W. M. Kak Laboratory of Hydraulics and Water Resources, California Institute of Technology; 1977.
[64] Poreh M, Kacherginsky A. Simulation of plume rise using small wind-tunnel models. J Wind Eng Ind Aerodyn 1981;7:1–14.
[65] Davidson GA. Simultaneous trajectory and dilution predictions from a simple integral plume model. Atmos Environ 1989;23(2):34–49.
[66] Becker BR, Stewart JR, Walter TM. A numerical model of cooling tower plume recirculation. Math Comput Model 1989;12(7):799–819.
[67] Johnston CR, Wilson DJ. A vortex pair model for plume downwash into stack wakes. Atmos Environ 1997;31(1):13–20.
[68] Snyder WH, Lawson RE. Fluid modeling simulation of stack-tip downwash for neutrally buoyant plumes. Atmos Environ 1991;25A:2837–50.
[69] Overcamp TJ, Israel GW. Sensitivity analysis of a salt deposition model for natural draft cooling towers. Atmos Environ 1978;13:61–9.
[70] Overcamp TJ. A general Gaussian diffusion-deposition model for elevated point sources. J Appl Met 1976;15:1167–71.
[71] König CS, Mokhtarzadeh-Dehghan MR. Numerical study out of three-dimensional, full-scale, turbulent, buoyant plumes from a multi-flue chimney in an atmospheric boundary layer. Atmos Environ 2002;36:3951–62.
[72] Mokhtarzadeh-Dehghan MR, König CS, Robins AG. Numerical study of single and two interacting turbulent plumes in atmospheric cross flow. Atmos Environ 2006;40:3909–23.
[73] Meroney RN. Protocol for CFD prediction of cooling-tower drift in an urban environment. J Wind Eng Ind Aerodyn 2008;96:1789–804.
[74] Wang SW, Wang JB, Burnett J. Mechanistic modeling of centrifugal chillers for HVAC system dynamics simulation. Build Serv Eng Res Technol 2000;21:73–83.